

zCOSMOS - 10k-bright spectroscopic sample ^{*}

The bimodality in the Galaxy Stellar Mass Function: exploring its evolution with redshift

L. Pozzetti¹, M. Bolzonella¹, E. Zucca¹, G. Zamorani¹, S. Lilly², A. Renzini³, M. Moresco⁴, M. Mignoli¹, P. Cassata^{5,6}, L. Tasca^{7,6}, E. Lamareille⁸, C. Maier², B. Meneux⁹, P. Oesch², D. Vergani¹, K. Caputi², K. Kovač², A. Cimatti⁴, O. Cucciati^{6,10}, A. Iovino¹⁰, Y. Peng², M. Carollo², T. Contini⁸, J.-P. Kneib⁶, O. Le Fèvre⁶, V. Mainieri⁹, M. Scodreggio⁷, S. Bardelli¹, A. Bongiorno⁹, G. Coppola¹, S. de la Torre⁶, L. de Ravel⁶, P. Franzetti⁷, B. Garilli⁷, P. Kampczyk², C. Knobel², J.-F. Le Borgne⁸, V. Le Brun⁶, R. Pelló⁸, E. Perez Montero⁸, E. Ricciardelli³, J.D. Silverman², M. Tanaka⁹, L. Tresse⁶, U. Abbas⁶, D. Bottini⁷, A. Cappi¹, L. Guzzo¹⁰, C. Halliday¹¹, A. Leauthaud⁶, A.M. Koekemoer¹², D. Maccagni⁷, C. Marinoni¹³, H.J. McCracken¹⁴, P. Memeo⁷, C. Porciani², R. Scaramella¹⁵, C. Scarlata¹⁶, and N. Scoville¹⁷

(Affiliations can be found after the references)

Received ---; accepted ---

ABSTRACT

We present the galaxy stellar mass function (*GSMF*) up to redshift $z \simeq 1$, based on the analysis of about 8500 galaxies with $I < 22.5$ (AB mag) over 1.4 deg², which are part of the zCOSMOS-bright 10k spectroscopic sample. We investigate the total *GSMF*, as well as the contribution of early- and late-type galaxies (ETGs and LTGs, respectively), defined by different criteria (broad-band Spectral Energy Distribution, morphology, spectral properties or star formation activities). We unveil a galaxy bimodality in the global *GSMF*, which shape is better represented by 2 Schechter functions, at least up to the $z \sim 0.55$, the maximum redshift at which we can explore the *GSMF* upturn due to our mass limit. The two mass regimes, respectively dominated by ETGs and LTGs, are a consequence of the bimodality observed in different galaxy properties. For the global population we confirm a mass-dependent evolution (“mass-assembly downsizing”), i.e. low-mass galaxies number density increases later and faster (by a factor of two between $z = 1$ and $z = 0$ for $\log(\mathcal{M}/\mathcal{M}_\odot) \sim 10.5$) than massive galaxies (by less than 15% for $\log(\mathcal{M}/\mathcal{M}_\odot) > 11$). We find that the *GSMF* evolution at intermediate-low \mathcal{M} ($\log(\mathcal{M}/\mathcal{M}_\odot) < 10.6$) is mostly explained by a growth in stellar mass driven by smooth and decreasing Star Formation Histories (SFHs), despite the redder colours predicted in particular at low redshift. The low/negligible evolution at higher \mathcal{M} sets a limit of 30-15%, decreasing with redshift and marginally with mass, to the fraction of major merging among the global galaxy population. From the analysis of different galaxy types, we find that ETGs, regardless of the classification method, increase in number density with cosmic time faster for decreasing \mathcal{M} , i.e. follow a top-down building history, with a median “building redshift” increasing with mass ($z > 1$ for $\log(\mathcal{M}/\mathcal{M}_\odot) > 11$) in contrast with hierarchical model predictions. For LTGs we find that the number density of blue or spiral galaxies with $\log(\mathcal{M}/\mathcal{M}_\odot) > 10$ remains almost constant with cosmic time from $z \sim 1$. Instead, the most extreme population of star forming galaxies (with high specific star formation), at intermediate/high-mass, is rapidly decreasing in number density with cosmic time. Our data can be interpreted as a combination of different effects. Firstly, we suggest a transformation, driven mainly by SFH, from blue active spiral galaxies of intermediate mass into blue quiescent and successively (1-2 Gyr after) into red passive types with low specific star formation. We find an indication that the complete morphological transformation, likely driven by dynamical processes, into red spheroidal galaxies, required longer time-scales or follows after 1-2 Gyr. A continuous replacement of blue galaxies is expected by low-mass active spirals growing in stellar mass. We estimate a growth rate in number and mass density of the red galaxies at different redshifts and masses. The corresponding fraction of blue galaxies which, at any given time, is transforming into red per Gyr, due to the quenching of their *SFR*, is on average $\sim 25\%$ for $\log(\mathcal{M}/\mathcal{M}_\odot) < 11$. We conclude that the build-up of galaxies and in particular ETGs follows the same downsizing trend with mass (i.e. earlier in high-mass galaxies) of the formation of their stars and opposite to that predicted by current SAM, with the role of major merging, if not marginal, not dominant ($< 30\%$) and decreasing with redshift and marginally with mass for $\log(\mathcal{M}/\mathcal{M}_\odot) > 10.6$ galaxies. We expect in such scenario a negligible evolution of the Galaxy Baryonic Mass Function (*GBMF*) for the global population at all masses and a decrease with cosmic time of the *GBMF* for the blue galaxy population at intermediate-high masses.

Key words. galaxies: evolution – galaxies: luminosity function, mass function – galaxies: statistics – surveys

1. Introduction

Tracing the history of the galaxy star formation (Lilly et al. 1996, Madau et al. 1996, Madau, Pozzetti, Dickinson 1998) and of stellar mass assembly (Dickinson et al. 2003) over the cosmic time represent the major efforts of modern cosmology. In particular, it is still uncertain how the

Send offprint requests to: Lucia Pozzetti e-mail: lucia.pozzetti@oabo.inaf.it

^{*} based on data obtained with the European Southern Observatory Very Large Telescope, Paranal, Chile, program 175.A-0839

bimodality seen in the local Universe in galaxies properties (colour, morphology, star formation and spectral features, Kauffmann et al. 2003, Baldry et al. 2004, Brinchmann et al. 2004) evolves and when it was built up. Galaxies in the local Universe show a clear bimodal colour distribution (Strateva et al. 2001, Hogg et al. 2002, Blanton et al. 2003) which suggests a different mechanism of evolution for galaxies lying on the two sequences (Menci et al. 2005; Scarlata et al. 2007b; De Lucia et al. 2007). Even if colour bimodality has been observed and studied also at higher redshift (Bell et al. 2004, Weiner et al. 2005, up to $z \sim 1$; Franzetti et al. 2007, Cirasuolo et al. 2007, up to $z \sim 1.5$; Giallongo et al. 2005, Cassata et al. 2008, Williams et al. 2009, up to $z \sim 2$), no study up to now has fully evaluated how the number densities of the two populations compare and evolve with cosmic time.

It is still unclear, indeed, how the Galaxy Stellar Mass Function (*GSMF*) is linked to the galaxy bimodality. Only recently Baldry et al. (2004, 2006, 2008) noted a ‘bimodal’ shape in the local *GSMF* in the SDSS with an upturn at masses lower than $10^9 M_{\odot}$, related to the two different galaxy populations. It is, therefore, extremely interesting to explore how such shape evolves with redshift and which mechanisms contribute to its appearance. From previous surveys it is well established that there is an increase/decrease of the fraction of red/blue or early/late type galaxies with cosmic time at intermediate masses since $z \sim 1$ (Fontana et al. 2004, Bundy et al. 2006, Arnouts et al. 2007, Scarlata et al. 2007b, Vergani et al. 2008), while it is still controversial the evolution in absolute number densities of the two populations, in particular for intermediate/massive galaxies. A knowledge of this evolution may help in constraining the nature of the quenching mechanism responsible for downsizing.

In agreement with the first formulation introduced by Cowie et al. (1996), a downsizing scenario in age and star formation history emerges in several observational studies i.e. most massive galaxies form their stars earlier and faster than lower mass ones (hereafter age-downsizing, Brinchmann & Ellis 2000; Gavazzi & Scodreggio 1996; Fontana et al. 2004, Kodama et al. 2004; Bauer et al. 2005; Feulner et al. 2005a,b; Juneau et al. 2005; Borch et al. 2006; Cucciati et al. 2006, Vergani et al. 2008). Age-downsizing is valid separately within each of the two populations producing galaxy bimodality, the red one (Thomas et al. 2005, Fontana et al. 2004) and the blue one (Noeske et al. 2007a,b). However, it is still unclear if it is coupled with a mass-assembly downsizing scenario for galaxy evolution and formation (Fontana et al. 2004, 2006; Pozzetti et al. 2003, 2007; Cimatti et al. 2006, Bundy et al. 2006), i.e. if the most massive galaxies assembled their mass earlier than lower mass ones. Furthermore, do low-mass galaxies contain younger stars and assemble later even within the same spectral type? The hierarchical model by De Lucia et al. (2006) predicts, for example, a bottom-up assembly history for elliptical galaxies (also called “upsizing”), following the hierarchical growth of dark matter haloes, in contrast to a top-down and downsizing scenario for the formation history of their stars.

A fundamental role towards answering these questions is played by deep surveys, sampling thousands of galaxies on large portions of the sky. Very deep surveys have been exploited to describe the shape of the stellar mass function at high redshift (Fontana et al. 2006; Drory et al.

2005; Gwyn & Hartwick 2005, Bundy et al. 2006, Pozzetti et al. 2007), but a clear picture on the stellar mass assembly and how it depends on the mass (mass-assembly downsizing) and galaxy types has not yet emerged. Previous studies have explored the evolution of different galaxy types in deep near-IR surveys, such as the K20, through the K-band Luminosity Function (Pozzetti et al. 2003) and the Galaxy Stellar Mass Function (Fontana et al. 2004), using spectral classification (i.e. absorption line galaxies vs. emission line galaxies), and more recently in larger optical and near-IR surveys such as the VVDS, COMBO17 and DEEP2, using colours or spectra to define galaxy types (Bell et al. 2004, Cimatti et al. 2006, Faber et al. 2007, Zucca et al. 2006, Arnouts et al. 2007, Vergani et al. 2008). Even if the results from different surveys are still controversial (compare for example Bell et al. 2004 and Cimatti et al. 2006 for the same dataset), most of these studies found that luminous and rather massive old galaxies were already quite common at $z \sim 1$ and their number density declines rapidly above this redshift. This suggests that merger events are ruled out as the major mechanism of their assembly history below $z \simeq 1$. However, the observational results on major merging and dry-merging are still contradictory (see Bell et al. 2006, van Dokkum 2005, Lin et al. 2004, de Ravel et al. 2009 and Renzini 2007 for a summary). On the other hand less luminous/massive ETGs decline in number density continuously with redshift (Cimatti et al. 2006). Scarlata et al. (2007b) show similar results also in the photometric survey COSMOS, using both the morphologically and the photometrically selected subsamples of early type galaxies. More uncertain is instead the evolution in number density of the most massive late type star forming galaxies.

Furthermore it is still strongly debated whether the evolution of the observed *GSMF* with cosmic time is mainly driven by merging events at any given mass, as predicted by hierarchical galaxy formation models (Cole et al. 2000, Menci et al. 2005, Bower et al. 2006, De Lucia et al. 2006, Monaco et al. 2006), or by the Star Formation Histories (SFHs, see Vergani et al. 2008, Walcher et al. 2008). Indeed, it was believed that galaxies were assembled via hierarchical mergers between massive cold dark matter haloes, in which baryonic star-forming matter was embedded. However, most of the hierarchical galaxy assembly models are not able to completely account for the observed *GSMF* and its evolution (see Fontana et al. 2004, 2006, Monaco et al. 2006, Caputi et al. 2006, Marchesini et al. 2008, Fontanot et al. 2009 for a detailed comparison with models). For instance, some models tend to underpredict the high-mass tail overpredict its evolution (Fontana et al. 2004, 2006), even in the extreme case of an evolution purely driven by mergers (Monaco et al. 2006). Only the the assumption that a significant fraction, $\sim 30\%$, of stars are scattered in the diffuse stellar component at each merger event leads to a significant suppression of the predicted evolution, in better agreement with observational constraints (Monaco et al. 2006). On the other hand most of them overpredict the low-mass end of the *GSMF* (see Fontana et al. 2006, Kitzbichler & White 2007, Marchesini et al. 2008i, Fontanot et al. 2009). Furthermore, the models do not correctly reproduce the downsizing trend in stellar mass observed in elliptical galaxies (Cimatti et al. 2006). Therefore, according to the last observational results, the current galaxy formation and evolutionary scenario is indeed changing towards one in which a smoother evolution

in mass growth and star-formation (due to accretion of cold gas) plays a major, if not dominant, role compared to dark matter (major) merging events.

In this paper we use the zCOSMOS spectroscopic survey (Lilly et al. 2007, 2009) for a comprehensive analysis of the *GSMF*. Compared to previous spectroscopic surveys, the relatively larger area and spectroscopic redshifts of zCOSMOS allows a higher precision, a better statistics and lower cosmic variance (Lilly et al. 2009), in particular for the massive end of the *GSMFs*. We derive the *GSMF* and its evolution with cosmic time since $z = 1$, as well as the contribution of different galaxy populations, using numerous classification methods, defined by their colours, morphologies, star formation activities or spectroscopic classifications. Thanks to the spectroscopic redshifts we can study the shape of the global *GSMF* with high precision, its evolution and how it is related to the bimodality in the galaxy properties (colours, morphologies, spectral properties) seen up to high redshifts. We explore the different role of major merging and SFHs as a function of \mathcal{M} and cosmic time to explain the observed *GSMF* evolution. We also explore the evolution with cosmic time of the *GSMF* of the different galaxy types and propose an evolutionary scenario.

Throughout the paper we adopt the cosmology $\Omega_m = 0.25$ and $\Omega_\Lambda = 0.75$, with $h_{70} = H_0/(70 \text{ km s}^{-1} \text{ Mpc}^{-1})$. Magnitudes are given in the AB system.

2. COSMOS and the bright 10k zCOSMOS spectroscopic sample

The Cosmic Evolution Survey (COSMOS, Scoville et al. 2007) is the largest HST survey (640 orbits) ever undertaken, imaging a field of $\sim 2 \text{ deg}^2$ with the Advanced Camera for Surveys (ACS) with F814W (Koekemoer et al. 2007). This survey was designed to probe galaxy evolution and the effects of environment up to high redshifts. COSMOS observations include a good coverage of the field with multiband photometry from the UV (with GALEX, Zamojski et al. 2007), optical (with Subaru and CFHT, Taniguchi et al. 2007, Capak et al. 2007), NIR (with CTIO, KPNO, Capak et al. 2007, and CFHT, McCracken et al. 2009) to MIR and FIR (S-COSMOS with Spitzer, Sanders et al. 2007), in combination with a multi-wavelength dataset from radio (with VLA, Schinnerer et al. 2007), millimeter (with MAMBO-2 at the IRAM telescope, Bertoldi et al. 2007), to X-rays (with XMM, Hasinger et al. 2007, and Chandra, Elvis et al. 2009).

The zCOSMOS spectroscopic survey (Lilly et al. 2007) is an ongoing ESO Large Programme (~ 600 hours of observations) aiming to map the COSMOS field with the VISible Multi-Object Spectrograph (VIMOS, Le Fèvre et al. 2003a), mounted on the ESO Very Large Telescope (VLT). The zCOSMOS survey is made of a *bright* part, with spectroscopy limited to objects in the magnitude range $15.0 < I < 22.5$, and of a *deep* part, which measures redshifts of $B < 25.25$ of galaxies colour selected to be in the range $1.4 < z < 3$, within the central 1 deg^2 . The bright part has already produced redshifts and spectra for about 10000 galaxies over $\sim 1.4 \text{ deg}^2$, the so called 10k-bright spectroscopic sample (Lilly et al. 2009), with an average sampling rate of about 33%. For more details on the zCOSMOS 10k-bright sample we refer to Lilly et al. (2009). Here we recall that the VIMOS spectroscopic observations

were done using the red medium resolution $R \sim 600$ MR grism (5550-9650 Å), the spectra have been reduced using the VIMOS Interactive Pipeline Graphical Interface software (VIPGI, Scodreggio et al. 2005) and redshift measurements were visually determined after a first hint provided by an automatic package (EZ, Garilli et al. in preparation). A quality flag was assigned to each redshift measurement. This flag ranges from 0 (failed measurement) to 4 (100% confidence level); flag 9 indicates spectra with a single emission line, for which multiple redshift solutions are possible. Further details on the quality flags and their spectroscopic verification probability to be correct are given in Lilly et al. (2009, see their Table 1). It should be noted that additional to the confidence classes described in Lilly et al. (2007), a decimal place (from 5 to 1, see Table 3 in Lilly et al. 2009) in the class indicates the level of consistency between the spectroscopic and photometric redshifts obtained through the Zurich Extragalactic Bayesian Redshift Analyzer (ZEBRA; Feldmann et al. 2006), using the optical to infrared SED.

2.1. The selected galaxy spectroscopic sample

The analysis presented in this paper is based on the zCOSMOS-10k bright sample (Lilly et al. 2009). From the total sample of 10644 objects observed spectroscopically, we used the objects within the statistical sample defined in the magnitude range $15 < I < 22.5$, and removed the spectroscopically confirmed stars, broad line AGNs, as well the galaxies with low quality redshift flag (flag < 1.5, i.e. with a verification rate < 90% and a spectroscopic redshift inconsistent with the photometric redshift). Moreover, in order to have a reliable SED fitting to multi-band photometric data, we have excluded objects with apparent magnitudes measured in less than 5 bands ($\sim 1.7\%$) and objects for which the ground photometry can be affected by blending of more sources, as derived from the number of ACS sources brighter than $I = 22.5$ within $0.6''$ ($\sim 0.5\%$). This results in 8450 galaxy spectra with secure spectroscopic measurements (7936 in the redshift range where the following analysis is carried out, $z = 0.1-1$), over 5045.80 arcmin^2 . Objects with redshift flags < 1.5 are taken into account statistically (see Section 5, Bolzonella et al. 2009 and Zucca et al. 2009 for details).

The final selected sample of 8450 galaxies, with highly reliable spectroscopic redshifts, has a complete multi-band photometric coverage (from UV to IRAC) and a morphological classification, along with the morphological parameters available, from the Zurich Estimator of Structural Types (ZEST; Scarlata et al. 2007a) and from Marseille estimates (Cassata et al. 2008, Tasca et al. 2009, MRS hereafter).

2.2. Photometric data

The COSMOS field has been covered by multi-band photometry over a wide range of wavelengths. In this paper we will use the observed magnitudes in 10 photometric bands (CFHT u^* and K_s , Subaru B_J , V_J , g^+ , r^+ , i^+ and z^+ , and Spitzer IRAC at $3.6 \mu\text{m}$ and $4.5 \mu\text{m}$). The description of the photometric catalogs are given in Capak et al. (2007), Sanders et al. (2007) and McCracken et al. (2009). Following the same approach as in Capak et al. (2007, see their Table 13) the photometry has been optimized by applying fixed zero-point offsets in each bands to the observed

magnitudes in order to statistically reduce the differences between observed and reference magnitudes computed from a set of template SEDs, finding in general very similar offsets.

3. Estimate of the stellar masses

We have used the stellar masses (\mathcal{M}) estimated from the fit to the multicolour Spectral Energy Distribution (SED), using the observed magnitudes in 10 photometric bands from u^* to $4.5 \mu\text{m}$ (see Section 2.2), following the method described in Pozzetti et al. (2007). In a parallel paper, Bolzonella et al. (2009) describe the different methods used to compute stellar masses, based on different assumptions about the population synthesis models (Bruzual & Charlot 2003, BC03; Maraston 2005, M05; Charlot & Bruzual 2007, CB07) and the star-formation histories (SFHs): smooth exponentially decreasing or complex SFHs with the addition of secondary bursts. In Bolzonella et al. the associated uncertainties and degeneracies are also discussed (see also Fontana et al. 2004, Pozzetti et al. 2007, Marchesini et al. 2008). Here we just recall that the accuracy of the photometric stellar masses is overall satisfactory, with typical dispersions due to statistical uncertainties and degeneracies of the order of 0.2 dex. It is also worth noting that the addition of secondary bursts to a continuous star formation history produces systematically higher (up to 40% on average) stellar masses, while population synthesis models with TP-AGB phase (Maraston 2005, Charlot & Bruzual 2007) produce shifts up to ~ 0.2 dex towards lower \mathcal{M} . Finally, the uncertainty on the absolute value of the \mathcal{M} due to the assumptions on the *Initial Mass Function* (*IMF*) is within a factor of 2 for the typical *IMFs* usually adopted in the literature.

In this paper we have adopted the stellar masses derived with *Hyperzmass* (see Pozzetti et al. 2007), a modified version of the photometric redshift code *Hyperz* (Bolzonella et al. 2000). We have used smooth exponential decreasing SFHs ($SFR(t) \propto \exp(-t/\tau)$ with time scale $\tau = [0.1, \infty]$, and age $t = [0.1, 20]$ Gyr forced to be smaller than the Hubble time at each redshift). This parametrisation may be inappropriate for actively star forming galaxies (especially at high redshifts, Renzini 2009), because it assumes that all galaxies are caught at their minimum SFR. However, for the redshift range explored ($z < 1$) and for passively evolving galaxies this assumption does not affect appreciably the mass determinations. We have checked that delayed exponential star formation histories ($SFR(t) \propto t/\tau^2 \times \exp(-t/\tau)$) does not affect significantly the stellar masses estimates. In this study we adopted the Calzetti et al. (2000) extinction law, solar metallicity (see also Table 1 in Pozzetti et al. 2007), Bruzual & Charlot (2003) population synthesis models and Chabrier *IMF* (Chabrier 2003) with lower and upper cutoffs of 0.1 and $100 M_{\odot}$, to which we refer hereafter as defaults, if not specified otherwise. All the *GSMFs* have been computed also using M05 and CB07 population synthesis models. In particular we are aware that the estimate of ETGs stellar masses at high- z are particularly sensible to the TP-AGB phase of the stellar population around 1-2 Gyr, producing a shift to lower masses up to 0.2 dex (Maraston et al. 2006). In the redshift range sampled here ($0.1 < z < 1.0$) ETGs have on average older stellar population (Thomas et al. 2005) not dominated by TP-AGB in particular for massive objects.

At higher redshifts ($z > 1 - 1.5$) the effect of the TP-AGB phase in younger (1-2 Gyrs) ETGs become very important and should not be neglected. In our data (limited to $z < 1$) we find that also using M05 models our main results and conclusions remain almost unchanged and differences will be discussed in the text.

4. Galaxy classification

We use 5 different methods to classify into early- or late-type (ETGs and LTGs, hereafter) each galaxy, according to its colours, star formation activity, morphology or spectroscopy, as follows:

1. Photometric classification (red and blue galaxies):

We derived galaxy *Photometric Types* (\mathcal{PT}) from the best-fit to the multi-band photometry (from u^* to K_s band, see previous Section). Following Zucca et al. (2006), we used the empirical set of (62) SEDs described in Ilbert et al. (2006). These SEDs were derived interpolating between the four local observed spectra of Coleman et al. (1980, spanning from the old stellar population in M31 and M81 to Sbc, Scd, and Im SEDs) and two starburst SEDs from Kinney et al. (1996). These templates are linearly extrapolated to the ultraviolet ($\lambda < 2000 \text{ \AA}$) and near-infrared wavelengths using the GISSEL synthetic models (Bruzual & Charlot 2003). Galaxies have been divided in four types, according to their spectral energy distribution from UV to near-IR. These types correspond to the red E/Sa template ($\mathcal{PT}=1$), early spiral template ($\mathcal{PT}=2$), late spiral template ($\mathcal{PT}=3$) and irregular or starburst template ($\mathcal{PT}=4$). Using the VVDS spectroscopic survey Zucca et al. (2006) have verified statistically the consistency between this photometric classification and the average spectral properties. Using stacked spectra of all galaxies in each of the four types, they showed an increasingly bluer continuum with stronger emission lines moving from $\mathcal{PT}=1$ to $\mathcal{PT}=4$, confirming the robustness of this classification scheme.

In Fig. 1, we show the $U - B$ rest-frame colour distributions for the galaxies of our sample divided according to the *Photometric Types*. From this figure it is clear that the 4 different types have different colour distributions, even if they significantly overlaps. It is also evident that the colour bimodality present in the sample can be well represented dividing the sample according to their *Photometric type*: red galaxies which have $\mathcal{PT}=1$ (2103 objects, also called SED-ETGs hereafter) and blue galaxies which have $\mathcal{PT}= 2, 3, 4$ (6347 objects, SED-LTGs), respectively. In Fig. 1 we also show the colour-mass diagram which confirms that the *photometric classification* applied to the 10k-bright zCOSMOS sample is very well consistent with previous selections of red-sequence galaxies based on colour-luminosity diagrams (Bell et al. 2004 and Cimatti et al. 2006) and has the advantage of using the entire multi-band photometric coverage rather than only two bands. In principle, given the good multi-band coverage, the SED fitting is able to break the degeneracy between a dust extinguished star forming galaxy with a red but smooth SED and a passive old galaxy with a strong 4000 \AA break in its SED (Pozzetti & Mannucci 2000).

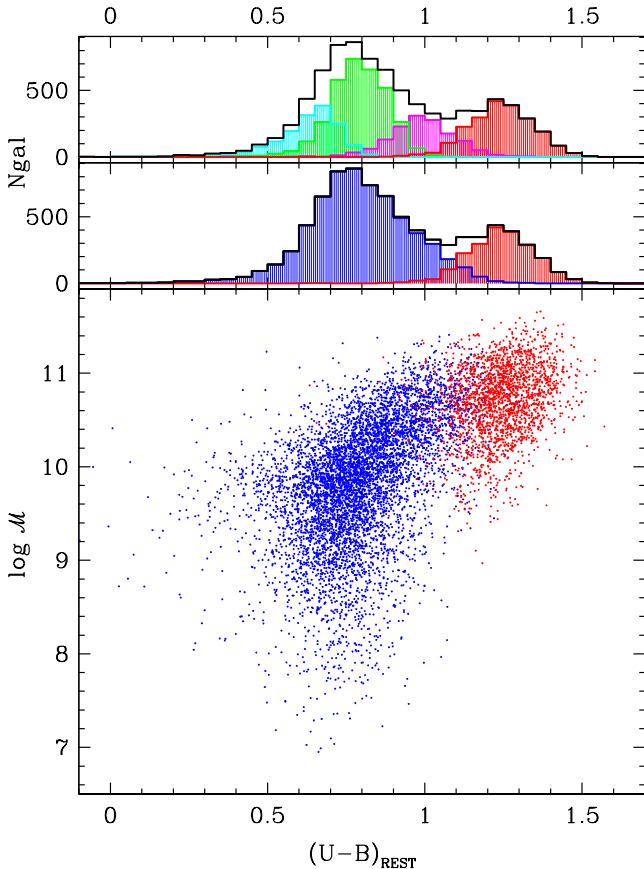


Fig. 1. The upper panels show the $U - B$ rest-frame colours distribution of galaxies with different *Photometric Types* (red for $\mathcal{PT}=1$, magenta for $\mathcal{PT}=2$, green for $\mathcal{PT}=3$, cyan for $\mathcal{PT}=4$, and blue for $\mathcal{PT}=2, 3, 4$, see text). The bottom panel shows the colour-mass diagram: red and blue colours represent SED-ETGs ($\mathcal{PT}=1$) and SED-LTGs ($\mathcal{PT}=2, 3, 4$), respectively.

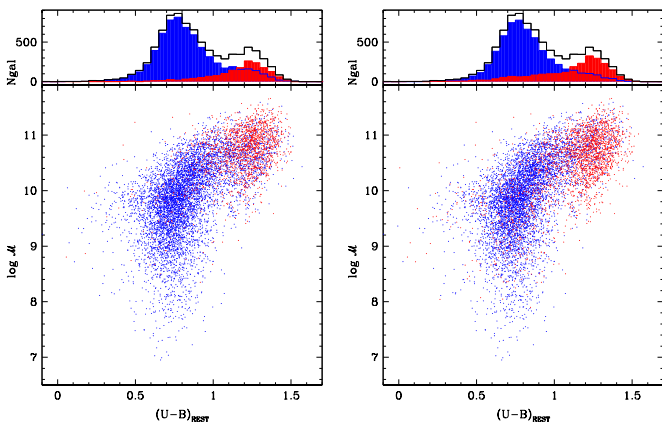


Fig. 2. $U - B$ rest-frame colours of galaxies with different morphological classes using ZEST (left panel) and MRS (right panel) classifications. The colour-mass diagrams are shown in the bottom panels: red and blue colours represent morpho-ETGs (spheroids) and morpho-LTGs (disc+irregulars), respectively.

2. Star Formation activity classification (active, quiescent and passive galaxies):

We divided the sample according to galaxy Star Formation Rate (SFR) activity. We used the SFR and the Specific Star formation Rate ($SSFR=SFR/M$) derived from the SED fitting (see previous Section), finding, in general, a good correlation between it and the $SSFR$ derived from [OII] (Maier et al. 2009) for galaxies in the redshift range $0.5 < z < 0.9$. We have, therefore, divided the sample into active and quiescent galaxies if $\log(SSFR/\text{Gyr}^{-1})$ is above or below -1 , i.e. galaxies which take less or more than 10 Gyr to double their M at the present SFR , respectively. We find in our sample 5051 active galaxies and 3403 quiescent galaxies. Note that with this definition the number of galaxies in the high $SSFR$ sample is $\sim 80\%$ of the blue galaxies as defined on the basis of the SED fitting. In addition, we further investigate the population of “passive” galaxies, i.e. 1612 galaxies with $\log(SSFR/\text{Gyr}^{-1}) < -2$.

3. Morphological classification (spheroidal and disc + irregular galaxies):

Taking advantage of the COSMOS HST+ACS images (Koekemoer et al. 2007), we divided the sample also using *morphological classes*. In order to take into account uncertainties on the morphological classification we used two of the available estimates, i.e. the Zurich Estimator of Structural Types (ZEST; Scarlata et al. 2007a) and a non-parametric estimate, derived in Marseille (MRS hereafter, Cassata et al. 2007, 2008, Tasca et al. 2009). Objects without a morphological classification are only a small fraction ($\sim 3-4\%$).

ZEST quantitatively describes the galaxy structure by performing a principal component analysis (PCA) in the five-dimensional parameter space of asymmetry (A), concentration (C), Gini coefficient (G), the second-order moment of the brightest 20% galaxy pixels (M20; Abraham et al. 2003), and the ellipticity of the light distribution (ϵ). The PCA indicates that the first three PC variables explain more than 90% of the variance in the original data set, thus almost completely describing the galaxy structure. The ZEST classification associates to each PC value a type (ZEST type, \mathcal{ZT} , =1 for early-type galaxies; =2 for disc galaxies; and =3 for irregular galaxies) and a “bulgeness” parameter according to the median value of the distribution of Sérsic indices n (Sargent et al. 2007) of all galaxies brighter than $I = 22.5$ (bulgeness=0,1,2,3, from $n > 2.5$ being bulge dominated to $n < 0.75$ being disc dominated galaxies). In this study, the total sample was divided into morpho-ETGs and morpho-LTGs, with the spheroidal sample including 1680 galaxies classified by ZEST as elliptical ($\mathcal{ZT}=1$, 759) or bulge-dominated ($\mathcal{ZT}=2.0$) galaxies, while the disc+irregular subsample includes 6413 galaxies (with \mathcal{ZT} greater than 2.0, i.e. from bulge-not-dominated to disc-dominated and irregular galaxies).

We have, in addition, used MRS morphological estimates. This classification scheme is done separating the galaxies on the basis of position in the multi-dimensional parameter space of the four non-parametric diagnostics of galaxy structures (C, A, G and axial ratio). First, the structural parameters are measured for all the galaxies in the sample. Then, a randomly extracted subset of 500 galaxies is visually classified (LT, PC) in ellipticals, spirals and irregulars. This reference

catalog is used to explore the multi-dimensional parameters space. For each new galaxy that needs to be classified, the distance in the parameter space to the 500 reference galaxies is measured, and the 11 closest are picked out. Finally, each galaxy is assigned to the most frequent visual class among these 11 nearest reference galaxies. This procedure allows to convert structural parameters into morphological classes: spheroidals (MRS type, $\mathcal{M}T=1$) spirals ($\mathcal{M}T=2$) and irregulars ($\mathcal{M}T=3$). In this paper we used, therefore, also this morphological classification to divide the sample into morpho-ETGs and morpho-LTGs, as for ZEST morphologies, having 2383 spheroidals ($\mathcal{M}T=1$) and 5831 disc+irregular ($\mathcal{M}T=2+3$) galaxies, respectively.

In Fig. 2 we show the $U - B$ rest-frame colour distributions and colour-mass diagrams for these different morphological classifications. In both morphological classifications there is a non-negligible number of blue spheroidal-type galaxies ($\sim 37\%$ in MRS and $\sim 29\%$ in ZEST) (see Section 8.2) as well as of red disc+irregular galaxies ($\sim 13\%$ in ZEST and $\sim 9\%$ in MRS).

4. *Spectroscopic classification (emission and absorption line galaxies):*

Using estimates of spectral features (Lamareille et al. in preparation) we have divided the sample in spectral-ETGs and spectral-LTGs following the criteria defined in Mignoli et al. (2009) for the zCOSMOS spectroscopic sample in the $EW_0[OII] - D4000$ plane: in the redshift range $0.55 < z < 1.0$ we find 1079 galaxies without strong emission lines and large 4000 Å break ($EW_0([OII]) < 5$ Å and $D4000 + 0.33 \log(EW_0([OII])) > 1.5$, spectroscopic type $\mathcal{S}T=1$, spectral-ETGs) and 3304 galaxies with strong emission lines and small 4000 Å break ($EW_0([OII]) > 5$ Å and $1.50 < D4000 + 0.33 \log(EW_0([OII])) < 2.22$, spectroscopic type $\mathcal{S}T=2$, spectral-LTGs), respectively.

5. *Combined classification: a clean sample of “bona-fide ETGs”:*

Finally, given the still controversial results based on morphology or colour-selected early-type galaxies (see Franzetti et al. 2007 for a discussion on colour-selected contamination), we have further defined a more conservative sample of “bona-fide ETGs” combining different criteria using colours, morphologies and spectral properties: from the sample of red galaxies (with *Photometric Type*=1) we have selected only those which are best fitted with the 4 reddest templates ($\sim 70\%$) and removed galaxies with strong emission lines ($EW_0([OII])$ or $EW_0(H_\alpha) > 5$ Å, $\sim 30\%$) or secure disc+irregular morphologies (using the intersection between MRS and ZEST estimates, $\sim 20\%$) or strong emission at $24 \mu\text{m}$ ($K - m(24\mu\text{m}) > -0.5$, $\sim 5\%$), obtaining a final sample of 981 red passive spheroidals (“bona-fide ETGs”). For further details see Moresco et al. (2009).

5. The Galaxy Stellar Mass Function

5.1. The method

To derive the Galaxy Stellar Mass Function (*GSMF*) we follow the traditional techniques used for the computation of the luminosity function. Here we apply the classical non-parametric $1/V_{\text{max}}$ formalism (Schmidt 1968) and estimate the best-fit Schechter (1976) parameters ($\alpha, \mathcal{M}^*, \phi^*$). In

performing the fit we allow up to 2 Schechter function components.

In order to correct for both the non-targeted sources in spectroscopy and those for which the spectroscopic measurement failed, we use a statistical weight associated with each galaxy with a secure redshift measurement. This weight is the inverse of the product of the *Target Sampling Rate* (TSR) times the *Spectroscopic Success Rate* (SSR). Accurate weights have been derived by Bolzonella et al. (2009, see also Zucca et al. 2009) for all objects with secure spectroscopic redshifts, taking into account the magnitude, colour and redshift dependence of the SSR, as well as the objects observed as compulsory ($\sim 2\%$) and the secondary objects ($\sim 2\%$) in the slits, which have different TSR from the whole sample.

5.2. The limits in mass

In a magnitude limited sample, the minimum detected stellar mass depends on the redshift and on the stellar \mathcal{M}/L ratio. This latter ratio obviously depends on the stellar populations and therefore on galaxy colours. To account for this limit we define at each redshift a minimum mass, \mathcal{M}_{min} , above which the derived *GSMF* is essentially complete because all types of galaxies are potentially observable above this mass.

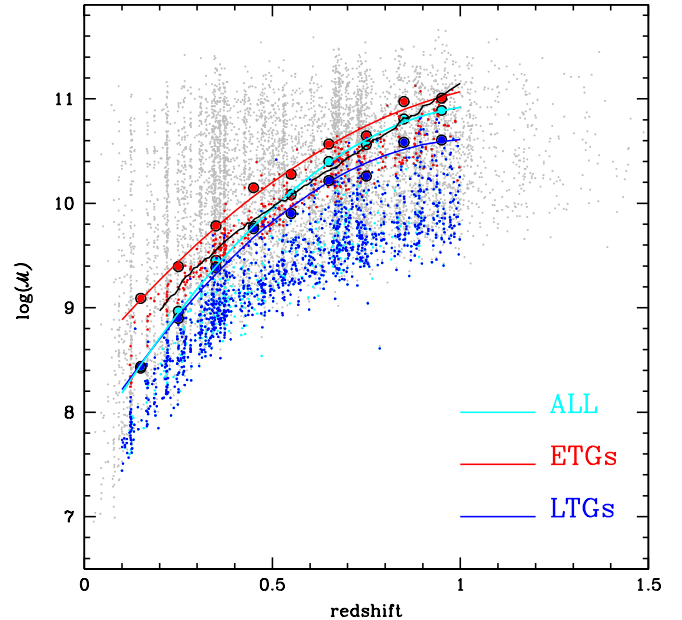


Fig. 3. Stellar mass as a function of redshift (small grey dots). Also shown are \mathcal{M}_{lim} (small coloured dots) and \mathcal{M}_{min} (big circles and lines in colour) at 95% of \mathcal{M}/L ratio completeness level (see text): cyan for the total population, red and blue colours for SED-ETGs and SED-LTGs, defined by their *Photometric Type*. Also shown in black the \mathcal{M} threshold (corresponding to 95% of completeness for the global *GSMF*) derived using mock Millenium samples by Meneux et al. (2009).

To derive \mathcal{M}_{min} we calculate for each galaxy the limiting stellar mass (\mathcal{M}_{lim}), i.e. the mass it would have, at

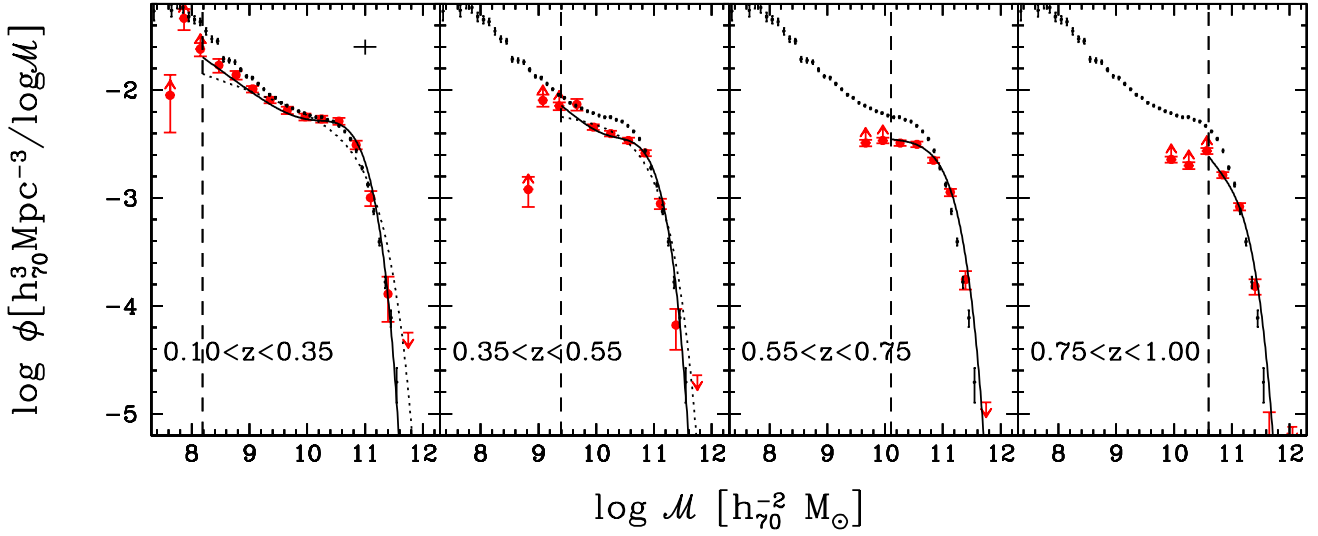


Fig. 4. Global Galaxy Stellar Mass Functions in four different redshift bins. Red points represent $1/V_{\max}$ determination and Poisson associated errors, while lines represent the Schechter fits. The global *GSMFs* are not well reproduced by one single Schechter function (dotted lines), but by two Schechter functions (continuous lines) up to $z = 0.55$. In the first two redshift bins the *GSMFs* show the inflection points of the bimodality around $\mathcal{M} \sim 5 \times 10^9 M_{\odot}$. The dashed vertical lines represent the mass limit in the corresponding redshift bin (\mathcal{M}_{\min}). Data are plotted as lower limits below \mathcal{M}_{\min} . Upper limits at 1σ (i.e. 1.84 objects) are shown at the high-mass end. Small black dots in all panels represent the local *GSMF* by Baldry et al. (2008). The cross at the right top of the first panel shows an estimate of the cosmic variance and mass uncertainties.

its spectroscopic redshift, if its apparent magnitude was equal to the limiting magnitude of the survey ($I_{\text{lim}} = 22.5$): $\log(\mathcal{M}_{\text{lim}}) = \log(\mathcal{M}) + 0.4(I - I_{\text{lim}})$. The result is a distribution of the limiting stellar masses, \mathcal{M}_{lim} , which reflects the distribution of the stellar \mathcal{M}/L ratio at each redshift in our sample. In order to derive a representative limit for our sample we use the \mathcal{M}_{lim} of the 20% faintest galaxies at each redshift. This choice takes into account the colour-luminosity relation and therefore includes only galaxies with typical \mathcal{M}/L near the magnitude limit. Doing that, we avoid to use an artificially too stringent limit due to the brightest and reddest (with the highest \mathcal{M}/L) galaxies, which are not significantly contributing near the magnitude limit of the survey. Figure 3 shows the distribution of the stellar masses for all galaxies and of the \mathcal{M}_{lim} for the 20% faintest galaxies. We then define $\mathcal{M}_{\min}(z)$ as the upper envelope of the \mathcal{M}_{lim} distribution below which lie 95% of the \mathcal{M}_{lim} values at each redshift. This \mathcal{M}_{\min} , which corresponds to a 95% completeness limit at each redshift in \mathcal{M}/L ratio observable at the limit of the survey, has been taken as the completeness limit for the *GSMF*. Meneux et al. (2009) instead made use of mock survey samples to derive the mass limit. The completeness is then simply defined, for a given redshift range and mass threshold, as the ratio of the number of galaxies brighter than the observed flux limit over those at any flux. Interestingly, even if this method is model-dependent, this approach leads to a similar completeness limit as the previous one. For example, for the global population we find that our \mathcal{M}_{\min} are in fairly good agreement with the 95% completeness limit (black curve in Fig. 3), derived by Meneux et al. (2009) for zCOSMOS, in most of the redshift range, and in any case the completeness for $\mathcal{M} > \mathcal{M}_{\min}$ is never lower than 85% at any redshift.

We have derived \mathcal{M}_{\min} at each redshift and for each galaxy sub-sample used. For the global population we note that \mathcal{M}_{\min} at low redshift is close to the limit for the bluest population (see Fig. 3), because blue galaxies dominate the zCOSMOS population close to the magnitude limit at that redshift, while the global \mathcal{M}_{\min} shifts towards the one of the reddest population at high redshift (at that redshift a significant number of red galaxies is present at the limit of our survey, and they have a higher \mathcal{M}/L ratio and therefore higher mass limit).

The derived *GSMFs* using the $1/V_{\max}$ technique, which further corrects for volume incompleteness, are formally complete for $\mathcal{M} \geq \mathcal{M}_{\min}(z_{\text{inf}})$, i.e. \mathcal{M}_{\min} at the lowest redshift of the considered bin. In the parametric fit we estimate the best-fit Schechter parameters using data above $\mathcal{M}_{\min}(z_{\text{inf}})$ and plotting as lower limits the data below \mathcal{M}_{\min} , where the *GSMFs* are incomplete. In addition we have taken into account upper limits above the maximum mass found in each considered redshift bin, deriving 1σ upper limits following Gehrels (1986) for the case of Poisson statistic for $n = 0$ events (i.e. ≤ 1.84 at 1σ).

6. The bimodality in the zCOSMOS global Galaxy Stellar Mass Function

The resulting *GSMFs* of the zCOSMOS galaxy sample are derived in the redshift range $0.1 < z < 1$. We have divided this redshift range into 4 redshift bins in order to have an approximately comparable number of objects in each redshift bin. This choice also dilutes the most prominent large scale structures present at different redshifts (Lilly et al. 2009, Kovač et al. 2009). Using the deviations from the median number densities in numerous redshift bins, affected by

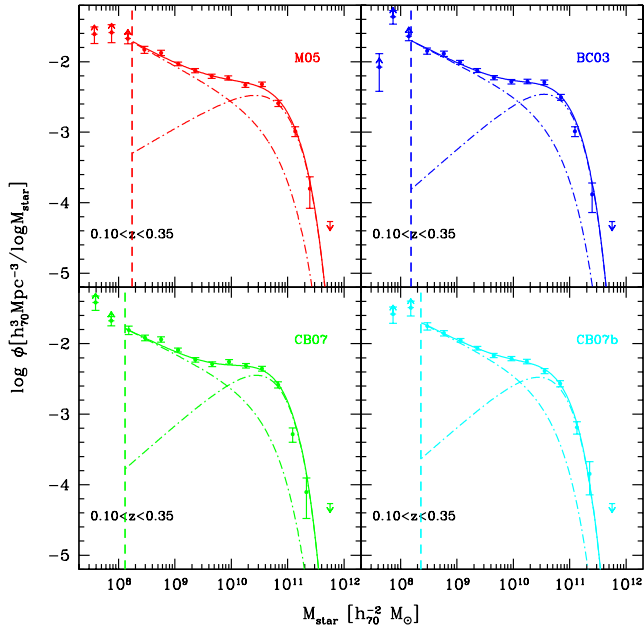


Fig. 5. Global *GSMF* in the first redshift bin using different SFHs and population synthesis models to derive the stellar masses (BC03, M05, CB07, CB07b=CB07+ secondary burst). Points and lines have the same meaning as in Figure 4. The dot-dashed lines represent the 2 Schechter components: they intersect around $\mathcal{M} \simeq 10^{10} M_{\odot}$.

different structures, we estimate that the systematic error on our *GSMFs* due to the cosmic variance is about 15-20%.

Figure 4 shows the global *GSMFs* in different redshift bins, using the $1/V_{\max}$ technique with Poisson errors associated. The first clear evidence is that at $z < 0.55$ the global *GSMFs*, derived using the $1/V_{\max}$ technique, show a bimodal behaviour with an upturn with a steep slope below $\mathcal{M} \sim 10^{9.5} M_{\odot}$, and they are not well reproduced by a single Schechter. At higher redshifts the reduced mass range due to the increase of \mathcal{M}_{\min} does not allow us to explore the upturn in the low-intermediate mass regime. We have, therefore, allowed the fit to use up to two Schechter functions. We verified that the characteristic mass (\mathcal{M}^*) of the second Schechter, which dominates at low-mass, is not well constrained and consistent with the characteristic mass of the most massive Schechter function. Therefore, following Baldry et al. (2008), we use hereafter a double Schechter function with a single \mathcal{M}^* value, given by:

$$\phi(\mathcal{M}) d\mathcal{M} = e^{-\mathcal{M}/\mathcal{M}^*} \left[\phi_1^* \left(\frac{\mathcal{M}}{\mathcal{M}^*} \right)^{\alpha_1} + \phi_2^* \left(\frac{\mathcal{M}}{\mathcal{M}^*} \right)^{\alpha_2} \right] \frac{d\mathcal{M}}{\mathcal{M}^*} \quad (1)$$

where $\phi_{\mathcal{M}} d\mathcal{M}$ is the number density of galaxies with mass between \mathcal{M} and $\mathcal{M} + d\mathcal{M}$, and $\alpha_2 < \alpha_1$, so that the second term dominates at the lowest masses.

Using galaxies with $\mathcal{M} \geq \mathcal{M}_{\min}$ we find that the slope parameters of the 2 Schechter functions are significantly different. Using the F-test we find that the fit with two Schechter functions is better than the fit with a single function at $\geq 3\sigma$ confidence level in the first two redshift bins. We checked that our findings on the double Schechter shape are not due to the particular SFHs and set of population synthesis models used to estimate \mathcal{M} . This is shown in

Figure 5, where we plot the *GSMF* derived in the first redshift bin ($0.1 < z < 0.35$) using different SFHs and population synthesis models for mass estimates.

The strength of the bimodality in the global *GSMF* is due to the mutual ratio between the two Schechter functions dominating at the high and low-mass end, respectively. In Section 8 we explore if the populations of ETGs and LTGs can explain this bimodality in the *GSMF*.

Since many years there is evidence for a ‘faint-end upturn’ in the optical galaxy luminosity functions, whereby the luminosity function is found to rise steeply at about 3–5 magnitudes below the characteristic luminosity (L^*), both in clusters (Driver et al. 1994, Popesso et al. 2006) and in the field (Zucca et al. 1997, Blanton et al. 2005). Note, however, that the upturn is not always evident in all samples (Norberg et al. 2002). On the other hand, the existence of this upturn is less clear in the *GSMF*. Only recently Baldry et al. (2004, 2006, 2008) revealed a similar shape for the local *GSMF* in the SDSS with an upturn at masses below $\sim 10^9 M_{\odot}$. Baldry et al. (2008), converting the galaxy luminosity function of the rich galaxy clusters in the SDSS (Popesso et al. 2006), found an even more prominent upturn in their *GSMFs*, compared to the field *GSMF*. On the other hand, the existence of this upturn was not clear up to now in the *GSMFs* derived from the deep surveys, even if a substantial population of low-mass galaxies ($< 10^9 M_{\odot}$) at low redshift ($z \simeq 0.2$), composed of faint blue galaxies, has been recently noted in deep surveys as the VVDS (Pozzetti et al. 2007). We note, *a posteriori*, from a comparison with other *GSMFs* from deep surveys (VVDS, Deep2, MUSIC, GOODS, FDF, COMBO17), that also previous surveys (in particular MUSIC, Fontana et al. 2006, and COMBO17, Borch et al. 2006) show some hint of bimodality in the shape of the *GSMFs*, even up to $z \sim 1$ (see Fig. 10 in Pozzetti et al. 2007). Also Ilbert et al. (2009) found that the *GSMFs* in COSMOS using photometric redshifts cannot be reproduced well with a single Schechter, but the upturn is less evident than in zCOSMOS sample. This could be explained by the higher precision in \mathcal{M} determination due in particular to the use of spectroscopic redshift rather than photometric ones.

The dependence of the *GSMF* shape, in the zCOSMOS survey, on the galaxy environment, as seen in the local Universe (Baldry et al. 2006), is investigated in a parallel paper (Bolzonella et al. 2009). They found that the bimodality seen in the global mass function appears even stronger in high density environments.

In the following sections we study the evolution of the global *GSMF* and how its shape is related to the bimodality in the galaxy properties. We derive the contribution of the different galaxy types to the *GSMF* and to its bimodal shape, and we explore its evolution with cosmic time. In Section 7.2 we explore also how the evolution, due to SFHs, different in high and low mass galaxy populations, changes the shape of the *GSMF* bimodality.

7. The evolution of the Galaxy Stellar Mass Function

In this section we explore how the evolution of the global *GSMF* with cosmic time depends on galaxy mass. From Figure 4 a mass dependent evolution of the global *GSMFs* was already evident, with a massive tail present up to

$z = 1$, and a moderate but continuous rising with cosmic time of less massive galaxies, confirming previous studies (Fontana et al. 2006, Pozzetti et al. 2007). This mass dependent evolution suggest that most of the massive galaxies (“mass-assembly downsizing”). Figure 6 shows the number densities (ρ_N), as derived by the $1/V_{\max}$ method, for two different mass limits ($\log(\mathcal{M}/M_{\odot}) > 9.77, 10.77$ corresponding to $\log(\mathcal{M}/M_{\odot}) > 10, 11$ for a Salpeter (1955) IMF, often used in literature). We compare our results with literature data from recent high- z deep surveys (VVDS, DEEP2, GOODS-MUSIC, FORS Deep Field, COMBO17; see Pozzetti et al. 2007 for details and references), and for the local Universe (Cole et al. 2001, Bell et al. 2003, Baldry et al. 2008). The local values for zCOSMOS have been derived assuming an evolution from the lowest redshift bin to $z = 0$ (see next Section for details). zCOSMOS data are consistent with most of previous observations at $z < 1$ and have a better determination with smaller uncertainties. We confirm a continuous evolution in number density for $\log(\mathcal{M}/M_{\odot}) > 9.77$ increasing towards the local Universe, and a slightly milder evolution for $\log(\mathcal{M}/M_{\odot}) > 10.77$, negligible for $z < 0.7$ ($< 20\%$) and more rapid above this redshift ($< 60\%$ since $z \sim 1$).

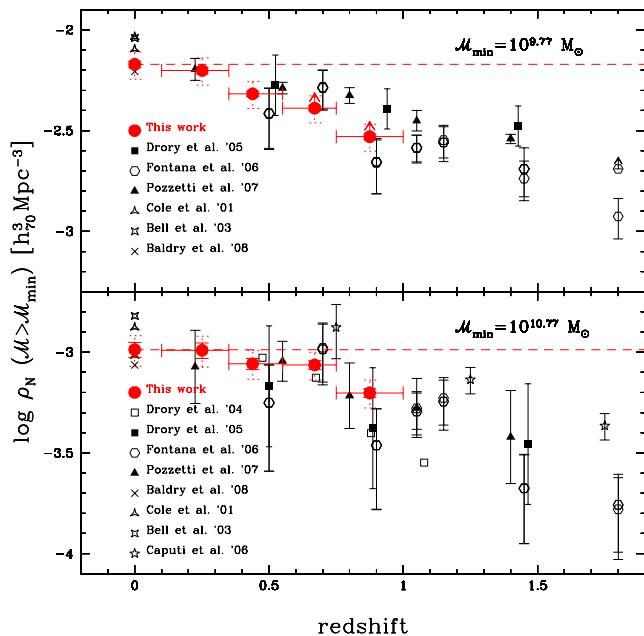


Fig. 6. Cosmological evolution of the galaxy number density as a function of redshift, derived using $1/V_{\max}$ from the zCOSMOS for 2 different mass thresholds ($> 10^{9.77} M_{\odot}$ and $> 10^{10.77} M_{\odot}$ from top to bottom). Dotted errors include cosmic variance estimates. zCOSMOS data at $z = 0$ have been derived from the “SFHs evolved *GSMFs*” (see Section 7 and Fig. 9). The dashed lines correspond to the no-evolution solution normalized at $z = 0$. Results from previous surveys (small black points) are also shown.

The same trend with mass is evident in Figure 7, which shows the number densities (ρ_N) as a function of redshift using a more extended range in mass limits (from $\log(\mathcal{M}/M_{\odot}) > 9$ to $\log(\mathcal{M}/M_{\odot}) > 11.3$). Over the en-

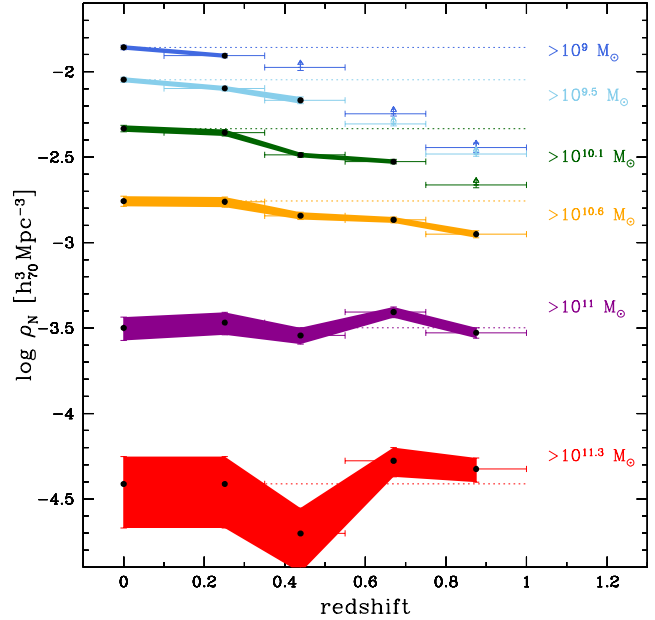


Fig. 7. Number density evolution using different mass limits for stellar masses. zCOSMOS data at $z = 0$ have been derived from the “SFHs evolved *GSMFs*” (see Section 7 and Fig. 9). The dotted lines correspond to the no-evolution solution normalized at $z = 0$.

tire mass range our data are consistent with a faster and steeper increase of the number densities with cosmic time going from high to low-mass galaxies: for comparison the evolution from $z = 0.44$ to $z = 0$ is 0.12 ± 0.02 dex for $\log(\mathcal{M}/M_{\odot}) > 9.5$ and 0.09 ± 0.03 for $\log(\mathcal{M}/M_{\odot}) > 10.6$. Only galaxies with $\log(\mathcal{M}/M_{\odot}) > 11$ show negligible evolution from $z = 1$ to the present time (0.03 ± 0.07 dex), while the evolution is 0.19 ± 0.03 dex for $\log(\mathcal{M}/M_{\odot}) > 10.6$, the lowest mass for which we are complete over the whole redshift range.

We can, therefore, confirm that the mass is an important factor to drive galaxy evolution. zCOSMOS data are consistent with a mass dependent assembly history, with most massive galaxies evolving earlier than lower mass galaxies (mass-assembly downsizing). On the basis of hierarchical galaxy formation models, one would expect that the evolution of individual galaxies is determined by numerous independent factors such as star forming history, merger history, mass, angular momentum, size and environment. The relative importance of the stellar mass and of the galaxy environment in the *GSMF* is investigated for the zCOSMOS dataset in a parallel paper (Bolzonella et al. 2009). They found that the evolution of the fractional contribution of different galaxy types to the environmental *GSMF* appears to be a function of overdensity in which the galaxy lives, and consistent with an accelerated trend of downsizing in overdense regions.

A detailed comparison of the global *GSMF* with hierarchical Semi Analytical Models (SAM) is postponed to a future paper. In Section 9 we compare some SAM models with ETGs observed *GSMFs*. Here we remind that most of the hierarchical galaxy assembly models are not able to completely account for the observed *GSMF* and its evolution (see Fontana et al. 2004, 2006, Caputi et al.

2006, Kitzbichler & White 2007, Marchesini et al. 2008, Fontanot et al. 2009 for a detailed comparison with models), which underpredict the high-mass tail and overpredict the low-mass end of the *GSMF*. Some new physical treatment of the baryonic component, such as the star formation history/timescale, feedback, dust content, AGN feedback (Menci et al. 2006, Monaco et al. 2007, Bower et al. 2006), and the uncertainties on mass determination, are able to reduce the disagreement (Kitzbichler & White 2007, Cattaneo et al. 2008, Fontanot et al. 2009). Fontanot et al. (2009) compare a broad compilation of available data-sets with the predictions of three different semi-analytic models of galaxy formation within the Λ CDM framework. They find that the main contributors, at all redshifts, to the low mass-end observed excess in the models are central galaxies in low mass dark matter haloes ($10^{11} < M_{\text{halo}}/M_{\odot} < 10^{12}$). They find also that, when observational errors on stellar mass are taken into account, the models acceptably reproduce massive galaxies ($\log(M/M_{\odot}) > 11$), but lower mass galaxies ($\log(M/M_{\odot}) = 9 - 10$) are formed too early in the models and are too passive at late times. Thus, the models do not correctly reproduce the downsizing trend in stellar mass. We show in Section 9 that, however, the typical uncertainties in the mass determination cannot completely explain the observed excess of massive galaxies compared to some hierarchical model predictions, and, when applied, the models tend to overestimate the high-mass galaxy number density at low-redshift (see also Fig. 1 in Fontanot et al. 2009).

In the following section we analyze whether the evolution of the observed *GSMF* with cosmic time is mainly driven by merging events at any given mass or by the SFHs.

7.1. A limit to the galaxy merging

The small evolution observed in the *GSMF* argues against a dominant contribution of galaxy mergers to galaxy evolution. If merger events, indeed, were efficient to form the most massive galaxies at $z < 1$ (as predicted by hierarchical models), we should expect instead a detectable increase in the number density of massive galaxies. In particular, the negligible evolution in the *GSMF* and in ρ_N for $\log(M/M_{\odot}) > 11$ galaxies up to $z \simeq 1$ suggests that they have formed and assembled their stellar mass at higher redshifts, ruling out “mergers” as the major mechanism of their mass assembly below $z < 1$. We find that less than 15% of the stellar mass density in present day galaxies with $\log(M/M_{\odot}) > 11$ has been accreted since $z \sim 1$, and less than 40% for $\log(M/M_{\odot}) > 10.6$. These values should be considered as upper limits to the mass accretion due to merging processes.

Here we derive the fraction of major mergers per Gyr consistent with the growth rate in number densities ($\delta\rho_N/\delta t = (\rho_N(z_{\text{sup}}) - \rho_N(z_{\text{inf}}))/\Delta t(z_{\text{sup}}, z_{\text{inf}})$, where ρ_N is evaluated using $1/V_{\text{max}}$ method)) at different \mathcal{M} . We define the fraction of “major merging” as:

$$f_{\text{merging}}(\mathcal{M}) = X \times \frac{(\delta\rho_N/\delta t)(\mathcal{M} * R)}{\rho_N(\mathcal{M})} \text{Gyr}^{-1}, \quad (2)$$

where X accounts for the number of galaxies in the mass bin that are involved in 1 merger and $\mathcal{M} * R$ is the total mass involved in 1 merger. We derive f_{merging} for $(X, R) = (2, 2), (1, 5/4)$ for the case of mergers with mass ratio 1:1

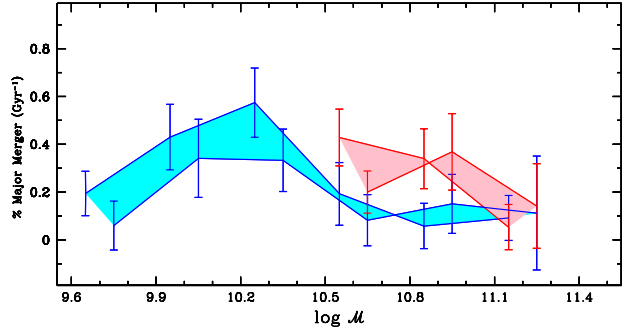


Fig. 8. Upper limits for the fraction of major merging per Gyr necessary to explain the growth rate in number densities of the global *GSMF* at any given \mathcal{M} (see text). Red and blue lines and uncertainties refer to two redshift: between the last two redshift bins ($z \sim 0.75$) and between the first two redshift bins ($z \sim 0.35$). They are plotted only for $\mathcal{M} > \mathcal{M}_{\text{min}} \simeq 10^{10.6, 9.6} M_{\odot}$, respectively. Shaded regions cover the two cases of mergers with mass ratio 1:1 and 1:4, as defined in eq. 2.

and 1:4, respectively. The results are shown in Figure 8 at two redshifts: between the last two redshift bins ($z \sim 0.75$) and between the first two redshift bins ($z \sim 0.35$) for galaxies above the $\mathcal{M}_{\text{min}}(z)$ (i.e. $\log(M/M_{\odot}) > 10.6$ and 9.6). We find at high redshift for massive galaxies a fraction always below $\sim 40\%$ decreasing to $\sim 10\%$ with cosmic time and marginally with mass at high- z . At low masses and redshifts there is a hint of an increase of the fraction for $\log(M/M_{\odot}) < 10.6$ up to $\sim 60\%$. These trends are consistent with the mass dependent evolution found in the evolution of the *GSMF*. Our result is consistent with the measure of a low major-merger rate of the most massive galaxies from galaxies pairs by de Ravel et al. (2009) in the VVDS. On the contrary at low mass our limits are larger and not very constraining. We remind that these values should be considered as upper limits to the contribution of merging processes to the evolution of the *GSMF*, assuming merging as the only effect.

7.2. Evolution driven by the SFHs at $z < 1$?

Here, instead, we try to interpret the mass-dependent evolution with cosmic time found in the *GSMF*, i.e. the increase in number density at a given \mathcal{M} or the shift in \mathcal{M} at a given number density, only by a “pure growth in stellar mass” with cosmic time due to the mass-dependent stellar formation history of each galaxies (Thomas et al. 2005, Noeske et al. 2007a,b). In this way we can quantify the residual importance of merging events or other processes, after accounting for galaxy star formation activity which drives the growth in stellar mass with cosmic time. A “SFH driven evolution” has been also adopted by Bell et al. (2007), assuming a constant specific SFR between two adjacent redshift bins and an instantaneous return fraction of 45%.

In this paper we have derived for each galaxy the \mathcal{M} evolved following its SFH (exponentially decreasing) derived from the SED fitting. Indeed, the best-fit parameters of the stellar population models (such as the star formation history time scale τ and the age) derived from the observed

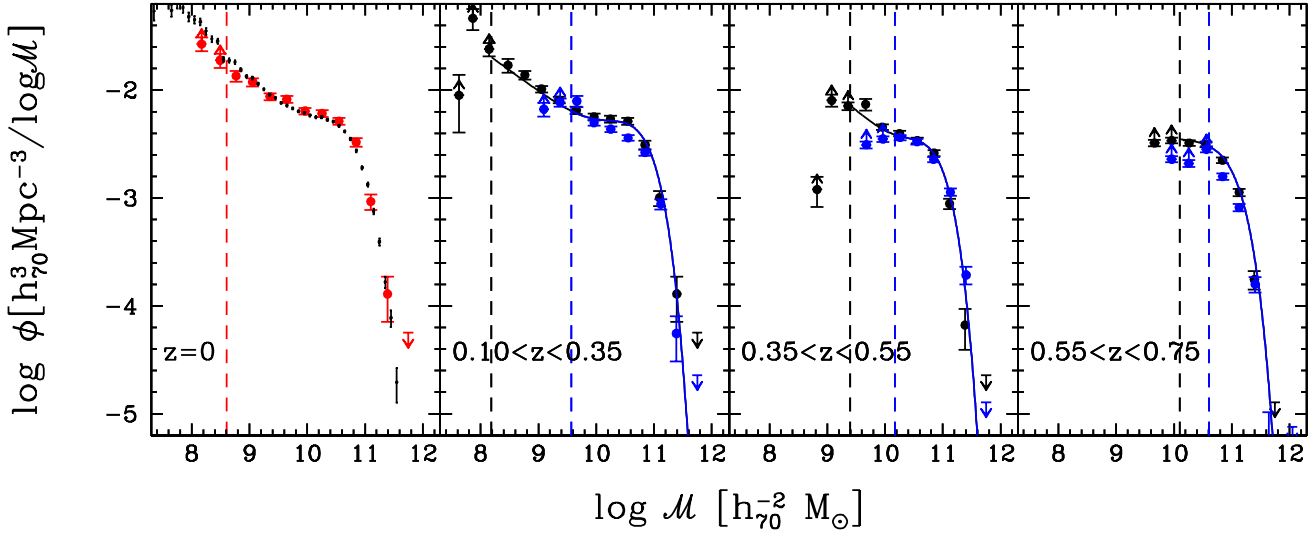


Fig. 9. “SFHs evolved *GSMF*” (blue points) compared to observed *GSMF* at redshift z (in black, from Figure 4). In the first panel we plot the *GSMF* evolved from the first redshift bin to $z = 0$ (red points). Vertical lines represent the respective mass limits. Red points are compared with the local *GSMF* (Baldry et al. 2008, shown as small dots).

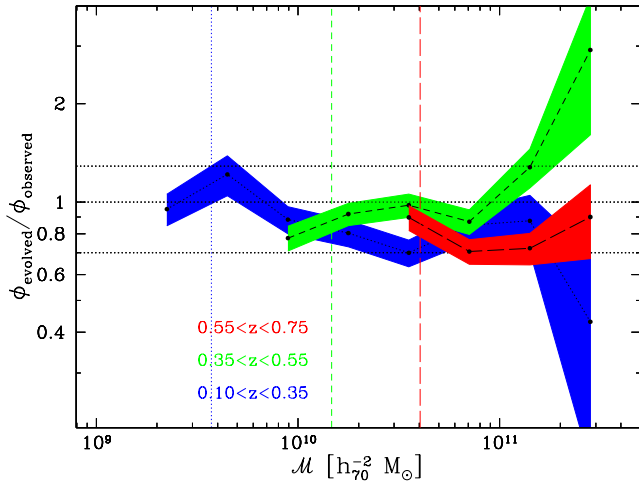


Fig. 10. Ratio between “SFHs evolved *GSMF*” and observed *GSMF* (both estimated using $1/V_{\max}$ technique) The dotted lines correspond to $\pm 30\%$ around 1.

SEDs, allow us to follow the evolution of stellar mass in cosmic time, under the minimum assumption that the galaxies evolved isolated (i.e. without merging) and continued to form stars in a smooth way with the same SFH derived from the SED fitting. For each galaxy at redshift z , we derived the \mathcal{M} evolved to the mean redshift of the previous (i.e. lower) redshift bin. The cosmic time elapsed between the mean redshifts of two adjacent redshift bins ranges between 1.1 and 1.6 Gyr. For galaxies in the lowest redshift bin ($z_{\text{mean}} = 0.25$) we have predicted the evolved \mathcal{M} to $z = 0$, i.e. after about 3 Gyr. We have made some simulations to test the reliability of this “evolved stellar mass” ($\mathcal{M}_{\text{evolved}}$): using models we create a simulated multi-band catalog (at the depth of our catalog, Bolzonella et al. 2000), from which we are able to recover not only the present \mathcal{M} of the input model (see also Pozzetti et al. 2007) but also

the model “evolved stellar mass”, after a given time; the agreement is overall satisfactory, with no systematic shifts and with typical dispersions due to statistical uncertainties and degeneracies of the order of 0.13 – 0.21 dex, depending on the elapsed time.

In Figure 9 we show the *GSMF* predicted at the average redshift of each bin using the galaxies in the higher redshift bin and compare it to the measured *GSMF* at the observed redshift. In the first panel we show also the *GSMF* predicted at $z = 0$ using galaxies in the first redshift bin ($0.1 < z < 0.35$).

First of all, we note a modest evolution from $z \simeq 0.25$ to $z = 0$, in particular for low/intermediate-mass galaxies ($\log(\mathcal{M}/M_{\odot}) < 10$) with a shift toward higher masses due to SFHs. The evolved *GSMF* approaches the observed local one (Baldry et al. 2008) and is rather consistent with it for $\log(\mathcal{M}/M_{\odot}) > 9$.

Within the zCOSMOS data we find a reasonable agreement at each redshift between “SFHs evolved *GSMF*” and the observed one at the same redshift. A raw agreement at $z > 0.3$ has been found by Bell et al. (2007) in the COMBO-17 assuming a constant SFH. Our result suggests that the *GSMF* evolution is, therefore, mostly driven by smooth and decreasing SFHs, due to the progressive exhaustion of the gas reservoir, for example from cold gas accretion, rather than by merger events or major bursts. Figure 10 shows the ratio between the evolved and the observed *GSMF*s in the first three redshift bins for $\mathcal{M} > \mathcal{M}_{\text{min}}$ of evolved galaxies. The agreement is good in particular at intermediate-low masses ($\log(\mathcal{M}/M_{\odot}) < 10.6$) where most of the *GSMF* evolution take place and therefore it could be explained mainly by the growth in mass driven by the SFHs in intermediate-low mass galaxies. At higher masses galaxies have low *SSFR* and therefore the SFHs are not able to explain the evolution observed in the MF, which in any case is quite small (see Figure 7). At high masses, therefore, the small *GSMF* evolution could be better explained by merging events, which involve in any case a low

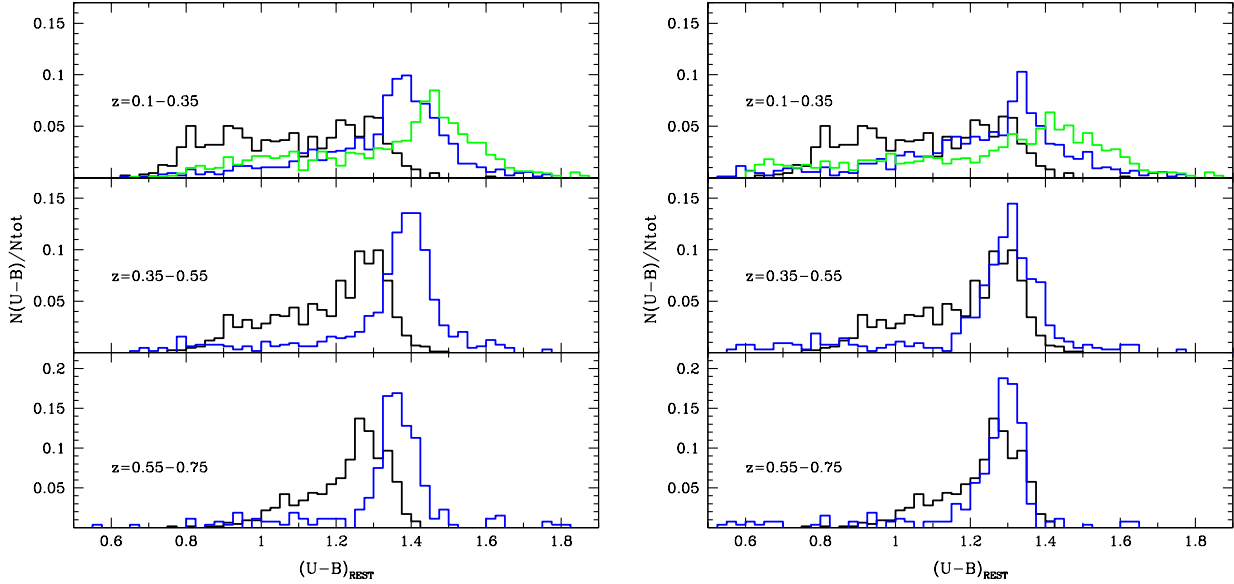


Fig. 11. Rest frame $U - B$ colour distribution in a mass limited sample (using the most conservative limit, see text) in different redshift bins, as observed (black histogram for the total population) and predicted using the “SFH evolution” from the next redshift bin (blue histogram). The green histogram in the top panels represent the expected $z = 0$ colour distribution by applying the “SFH evolution” to the galaxies in the first redshift bin. *Left panel:* assuming no evolution in the dust content, i.e. the same dust content derived from the SED fitting at the observed redshift; *right panel:* assuming no dust content in the evolved galaxies.

fraction of galaxies and decrease with redshift (see Figure 8). Oesch et al. (2009) further discuss the role of merging in the evolution of massive galaxies within the COSMOS survey.

At all masses we find at most differences of 20 – 40% between evolved and observed $GSMFs$. The residual differences could be retraced to different processes. Between them one solution is an additional SFR, i.e. more prolonged SFHs than derived from the SED fitting, or a different SFH functional form (Renzini 2009), or secondary bursts. Indeed from the SED fitting we find, for the blue galaxies, that the distribution of the time scale (τ) for the exponential SFHs has a median value of 1 Gyr, even if it presents an extended tail at higher values. This median value is quite short when compared to the value inferred from the global SFHs (the compilation of Hopkins & Beacom 2006 is consistent with $\tau \sim 3.5$ Gyr at $z < 1$). The mass growth from the SED fitting is on average about a factor 1.7 (0.24 dex) for $\mathcal{M}=10^{9.5} \mathcal{M}_\odot$ and 1.22 (0.09 dex) for $\mathcal{M}=10^{10} \mathcal{M}_\odot$, but it reaches up to a factor 30 for the most extreme star-forming galaxies, always with $\log(\mathcal{M}/\mathcal{M}_\odot) < 10$.

We have also checked if the predicted colour distributions for the “SFHs evolved galaxies” are consistent with the observed colour distributions at different redshifts. Figure 11 shows the expected colour distributions compared to the observed ones at different redshifts in the two extreme hypotheses about the dust content: (A) (left panel): no evolution in the dust content, i.e. assuming the same dust content derived from the SED fitting at the observed redshift, or (B) (right panel) no dust content in the evolved galaxies. In both panels we compare the colour-distribution for galaxies in a mass limited sample using the most conservative limit $\mathcal{M}_{\min}(z_{\text{sup}})$ for evolved masses. Model A predicts too red colours at all redshifts, while only the extreme

case of model B, i.e. without any dust content, is consistent with the observed colour distributions, at least at $z > 0.35$, while, in any case, it predicts too red colours at lower redshift. This could be related (again) to a too fast decreasing (quenching) of the SFHs of each galaxy as predicted by the SED fitting technique. Therefore we conclude that more extended SFHs or secondary bursts appear to be necessary to better reproduce the observed colours, in particular at low-redshift. One possibility could be to directly take into account the observed decreasing/quenching of the SFR at later cosmic time at progressively lower masses (see also Section 4). We postpone the discussion on this possibility to a future paper.

Residual differences between observed and “SFH evolved $GSMF$ ” are always lower than $\sim 40\%$, and even lower than 20% for $\log(\mathcal{M}/\mathcal{M}_\odot) < 10.3$. They could be also explained by merger events (see previous section) or other different dynamical processes which would induce a growth in stellar mass not related to the SFH. For instance the limit to the merging fraction, after accounting for the growth in mass due to the ongoing star formation in intermediate-low mass galaxies, could be reduced from 60% (Fig. 8) to less than 30-20% also for $\log(\mathcal{M}/\mathcal{M}_\odot) < 10.6$. We conclude therefore that the role of merging events is, if not marginal, not dominant ($< 30\%$) at any mass to explain the evolution of the $GSMF$. Very similar results on the role of the merger events (up to 20%) and a larger contribution to the mass growth rate by the less massive and star forming galaxies have been obtained independently also by Vergani et al. (2008) in the VVDS. We can compare our result with other independent measurements, e.g. of the merging rate from physically associated pairs of galaxies from spectra. de Ravel et al. (2009) measured the major merger rate from galaxies pairs with roughly equal mass

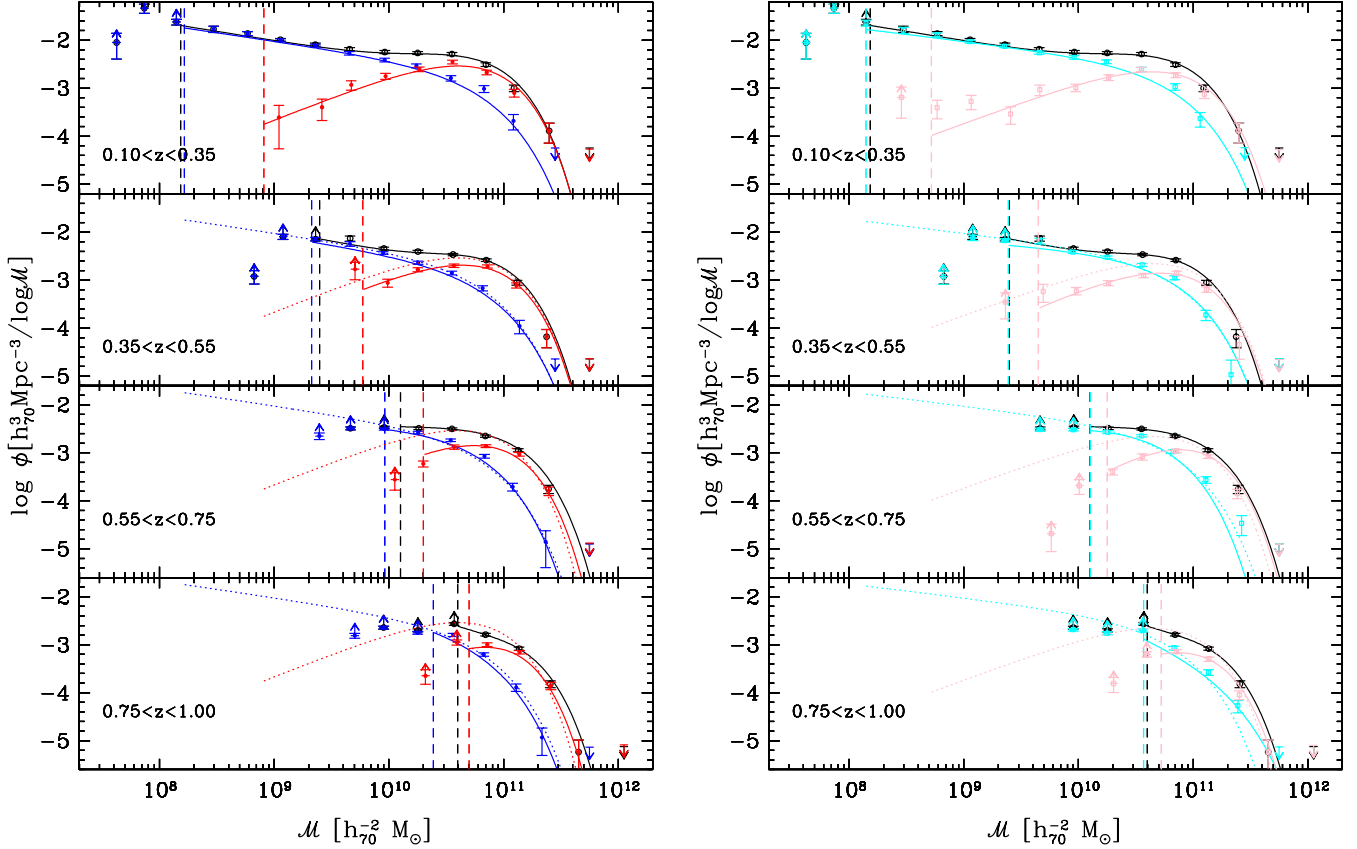


Fig. 12. Galaxy Stellar Mass Function by galaxy types. *Left panel:* *GSMFs* by *Photometric Types* ($PT=1$ in red, $PT=2+3+4$ in blue, total population in black). *Right panel:* *GSMFs* for *Morphological types* ($ZT=1,2,0$ in pink and $ZT_i:2,0$ in cyan) In both panels points represent the $1/V_{\max}$ determination, while continuous lines the Schechter fits. Dotted lines reported in each panel, as a reference, are the Schechter fits in the first redshift bin. Dashed vertical lines represent the mass limit in the corresponding redshift bin (\mathcal{M}_{\min}).

($\Delta M_B \leq 1.5$ mag) in the VVDS. In agreement with our results, they found that between 10 and 30% of the galaxies with $\log(\mathcal{M}/\mathcal{M}_\odot) > 9.5, 10.5$ are in pairs (see their Fig. 9).

8. Mass Functions by galaxy types

In order to explore the bimodality observed in the *GSMF* and how it progresses with time and with galaxy-type evolution, we derived a type-dependent *GSMF* using the different classifications described in Section 4.

Figure 12 (left panel) shows the *GSMF* as a function of *Photometric Types*, red ($PT=1$) versus blue ($PT=2,3,4$) galaxies; similar *GSMFs* are obtained using morphological criteria (right panel). We find that the red/spheroidal and blue/disc+irr populations show very different *GSMFs*, which can be linked to the bimodal shape seen in the global *GSMF*. Indeed, the massive end of the mass function ($\mathcal{M} > 10^{10.5} \mathcal{M}_\odot$) is mainly dominated by red/spheroidal galaxies up to $z = 1$, while blue/disc+irr galaxies mostly contribute to the intermediate/low-mass part ($\mathcal{M} < \mathcal{M}^*$) of the mass function at all redshifts. For $\log(\mathcal{M}/\mathcal{M}_\odot) > 11$ the number density of blue galaxies is always below $\sim 2 \times 10^{-4}$ gal/Mpc³/log \mathcal{M} .

We derived, using the $1/V_{\max}$ data points, the intersection of the *GSMFs* of the two populations ($\mathcal{M}_{\text{cross}}$). For the

photometric classification $\mathcal{M}_{\text{cross}}$ is at $\sim 1.9(\pm 0.2) \times 10^{10} \mathcal{M}_\odot$ in the first redshift bin and evolves with redshift, increasing by about a factor 2 (see red circles in Figure 13) at $z = 1$. A similar trend with redshift, although with somewhat higher values of $\mathcal{M}_{\text{cross}}$ are found using the *morphological classification* to divide the sample into spheroids and disc+irregular galaxies, for both classification schemes explored in this paper. Our results are consistent with previous determinations of $\mathcal{M}_{\text{cross}}$ in other deep surveys, such as the VVDS (Vergani et al. 2008) and the DEEP2 (Bundy et al. 2006), with the only exception for $\mathcal{M}_{\text{cross}}$ derived by Bundy et al. 2006 using morphological types (the highest line in Fig. 13). In this case the difference could be due to a different and more extreme definition of morphological ETGs, in Bundy et al. (2006). The extrapolation of our $\mathcal{M}_{\text{cross}}$ to $z = 0$ is also consistent with local results (Baldry et al. 2004, Bell et al. 2003).

The evolution of $\mathcal{M}_{\text{cross}}$ indicates an increase/decrease of the fraction of early/late galaxies with cosmic time at intermediate masses, as already noted in previous surveys (Fontana et al. 2004, Bundy et al. 2006, Arnouts et al. 2007, Scarlata et al. 2007b, Vergani et al. 2008). Oesch et al. (2009) found similar results within the COSMOS survey using accurate photometric redshifts. Bolzonella et al.

(2009) find a more rapid evolution of $\mathcal{M}_{\text{cross}}$ in high density environments.

The evolution in absolute number density of the two populations is instead still uncertain, in particular for the late type galaxies at intermediate-high \mathcal{M} . By comparing the zCOSMOS *GSMFs* in different redshift bins, we find that the evolution of $\mathcal{M}_{\text{cross}}$ is mainly due to a clear increase with cosmic time of the number density of red/spheroids of intermediate mass (around \mathcal{M}^* and below $10^{11} \mathcal{M}_{\odot}$), coupled with only a marginal evolution of the number density of blue/spiral galaxies at the same masses.

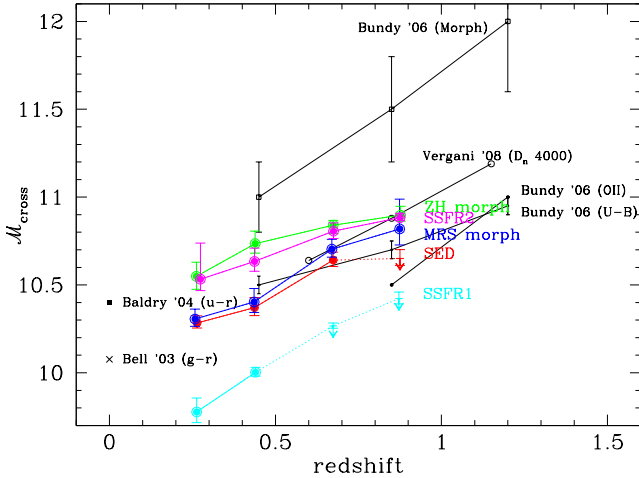


Fig. 13. The intersection of the *GSMFs* ($\mathcal{M}_{\text{cross}}$) of the two populations (ETGs and LTGs) as a function of redshift. Filled circles of different colours refer to the different classification schemes adopted and were derived from the $1/V_{\text{max}}$ estimate of the *GSMFs*; upper limits are shown where $\mathcal{M}_{\text{cross}}$ is lower than $\mathcal{M}_{\text{min}}(z)$. In black we show data from literature (references are marked, along with the respective classification criteria).

These trends are even more clear from the analysis of the number densities vs. redshift in different mass ranges ($\log(\mathcal{M}/\mathcal{M}_{\odot}) = 10 - 11.5$), derived using $1/V_{\text{max}}$ technique and shown in Figure 14. We find that the number density of massive ($\log(\mathcal{M}/\mathcal{M}_{\odot}) > 11$) red types is almost constant up to $z = 1$ (see also Pozzetti et al. 2003, Scarlata et al. 2007b, Ilbert et al. 2009) and dominates the total number density at these masses, while the number density of intermediate-mass ($10^{10} - 10^{11} \mathcal{M}_{\odot}$) red types increases with cosmic time. This increase is steeper at smaller masses. Between $z \simeq 0.45$ and $z \simeq 0.25$ it is 0.05 ± 0.08 , 0.14 ± 0.04 , 0.24 ± 0.05 dex for the three considered mass ranges ($\log(\mathcal{M}/\mathcal{M}_{\odot}) = 11, 10.5, 10$), respectively. This trend indicates a *mass-assembly downsizing* already noted in the global population and even more clear in the build-up of the red sequence (Cimatti et al. 2006).

Conversely, we find that the number density of late blue types with $\mathcal{M} > 10^{10} \mathcal{M}_{\odot}$ remains approximately constant with cosmic-time from $z = 1$. Their evolution in number density is less than 10 – 20% over the whole redshift and mass range (Figure 15 upper panel). These results are consistent with those of Arnouts et al. (2007), who find that the integrated stellar mass density of the active population shows only a modest mass growth rate, in contrast with an

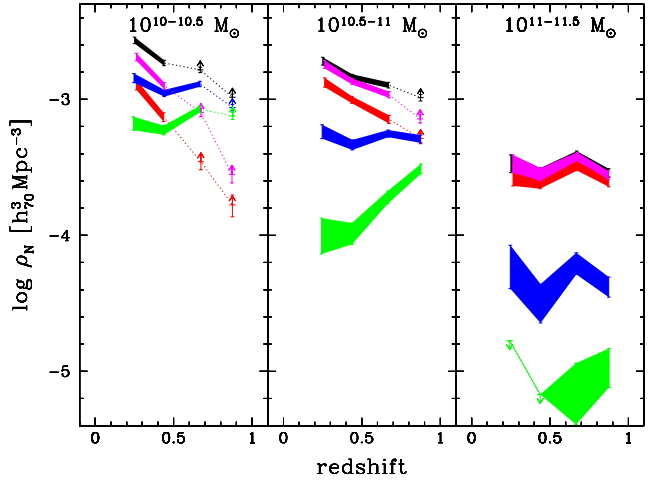


Fig. 14. Number density evolution in different mass ranges. Different colours refer to different population classes: black refers to the total population, red and blue to SED-ETGs and SED-LTGs using photometric classification, while magenta and green refer to low-*SSFR* and high-*SSFR* populations, respectively. Hatched regions refer to *GSMF* complete in the mass range and redshift considered, while dotted lines and lower limits are plotted at redshifts where the *GSMF* is not complete in the considered mass range.

increase by a factor of 2 for the quiescent population. Bundy et al. (2006) found that the abundance of blue galaxies declines by 0.1 – 0.2 dex from $z = 0.75 - 1.0$ to $z = 0.4 - 0.7$ at $\log(\mathcal{M}/\mathcal{M}_{\odot}) = 10.6 - 11.3$ (see their Fig. 6). A small evolution of the “blue cloud *GSMF*” is also found by Bell et al. (2007) in the COMBO-17 survey up to $z \simeq 0.9$.

How is this small/negligible evolution in the blue *GSMFs* related to the global decrease with cosmic time in the *SFR* density since $z \sim 1$ (see Hopkins et al. 2006) and to the downsizing in *SFR* (Cowie et al. 1996)? To answer these questions, we have analyzed the *GSMFs* of galaxies with different *SFR* activities. In particular we have derived the *GSMFs* for the most extreme star-forming population, i.e. those with high *SSFR*.

Using the estimates of the *SFR* and *SSFR* derived from the [OII] lines (Moustakas et al. 2006 calibration), Maier et al. (2009) find that very few zCOSMOS galaxies with masses above $\log(\mathcal{M}/\mathcal{M}_{\odot}) > 10.8$ have $1/SSFR$ s below the age of the universe at $0.5 < z < 0.7$, while there exist several dozens of galaxies above the same mass which are strongly star-forming at $0.7 < z < 0.9$ (see Fig. 2 in Maier et al. 2009). The same trend is observed using the *SFR* and *SSFR* derived from the fit to the multi-band photometry with synthetic models. Using SED fitting determination we note, first of all, that the median *SFR* and *SSFR* decreases with cosmic time in massive blue galaxies with $\log(\mathcal{M}/\mathcal{M}_{\odot}) > 10.5$ (for example the median $\log(SSFR/\text{Gyr}^{-1})$ is -1.0 at $0.7 < z < 1.0$, while it is -1.4 at $z < 0.3$) and with increasing mass limit from $\log(\mathcal{M}/\mathcal{M}_{\odot}) > 9.5$ to $\log(\mathcal{M}/\mathcal{M}_{\odot}) > 11$.

We have therefore derived the *GSMFs* using the *SSFR* derived from the SED fitting and dividing the sample as described in Section 4, i.e. with $\log(SSFR/\text{Gyr}^{-1})$ above or below -1, i.e. active and quiescent galaxies. Figure 15

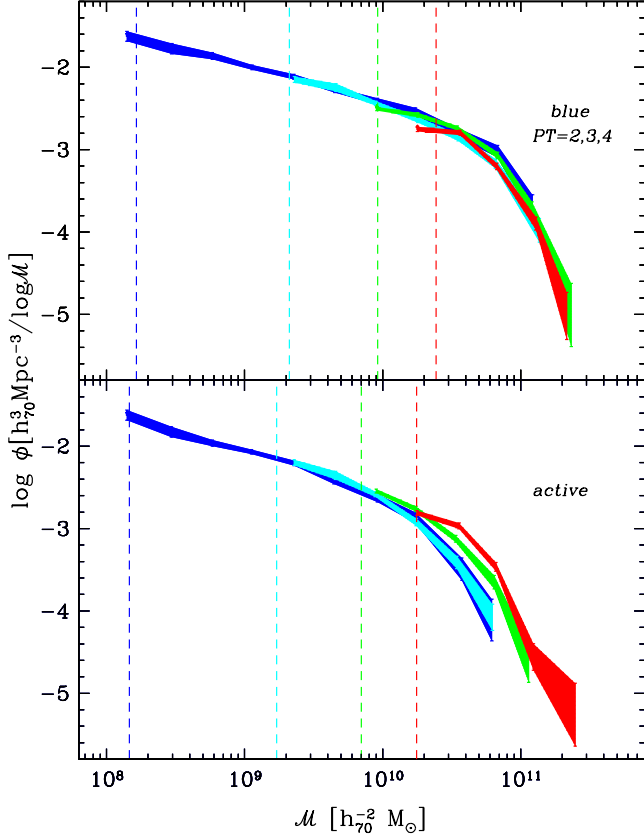


Fig. 15. *GSMFs* for LTGs using two classification schemes: blue galaxies ($PT=1$), active ($\log(SSFR/\text{Gyr}^{-1}) > -1$), as defined in Sec. 4. Only $1/V_{\max}$ determinations have been plotted, with their uncertainties. Different colours refer to different redshift ranges, increasing from blue ($0.10 < z < 0.35$), cyan ($0.35 < z < 0.55$), green ($0.55 < z < 0.75$) to red ($0.75 < z < 1.0$).

(lower panel) shows indeed a decrease with cosmic time of the *GSMFs* of the high-*SSFR* galaxies, in particular for $\log(M/M_{\odot}) > 10.3$. Their *GSMF* shows, indeed, a mass dependent evolution stronger at the massive end. In the highest redshift bin ($0.75 < z < 1$) the *GSMF* of the high-*SSFR* galaxies increases in number density and approaches that previously derived for the sample of blue (SED-LTGs) galaxies.

From the comparison of the *GSMFs* of the blue galaxies and the *GSMFs* of the high-*SSFR* galaxies we find that, while the number density of blue galaxies is approximately constant, it decreases significantly with cosmic time for high-*SSFR* massive objects (see Figures 14 and 15). From $z \sim 0.85$ to $z \sim 0.25$ the number density of high-*SSFR* active galaxies with $\log(M/M_{\odot}) > 10.5$ decreases by a factor ~ 3 (-0.49 ± 0.12 dex). Therefore the decrease with cosmic time of active massive galaxies is balanced by the constancy of intermediate-activity blue galaxies and the increase of intermediate mass quiescent and red galaxies. Zucca et al. (2009) studying the *B*-band Luminosity Function in zCOSMOS find results consistent with this scenario where a part of blue galaxies is transformed in red galaxies with increasing cosmic time.

Summarizing, these data suggest that we are witnessing a transformation with cosmic time from active into passive galaxies and a decrease (increase) in fraction with cosmic time of late (early) types. These changes in fraction are mostly due to the clear increase with cosmic time of the number density of intermediate mass ($M \sim 10^{10} - 10^{11} M_{\odot}$) early-type galaxies, while the density of intermediate mass blue or morpho-LTGs remains almost constant, always refilled by blue active galaxies of even lower masses. The median *SSFR* of blue massive galaxies decreases with cosmic time and with increasing mass. Therefore, blue high star-forming (with high *SSFR*) galaxies of intermediate-mass ($\log(M/M_{\odot}) = 10 - 11$) increase in mass and decrease in *SFR* or *SSFR* with cosmic time, transforming into low-*SSFR* blue objects and, quenching their *SFR*, into red passive objects ($\log(M/M_{\odot}) < 10$) increase in mass and replace in the *GSMFs* the blue intermediate-mass objects, whose density remains almost constant. In agreement with our results Bell et al. (2007), assuming a growth in stellar mass with a constant *SFR* equal to the instantaneous one (subtracting 45% of return fraction), found that the *GSMFs* of blue galaxies would be dramatically overproduced. Only assuming that all the growth in stellar mass is added to the red sequence they reproduced the evolution of the blue and red stellar mass functions with striking accuracy.

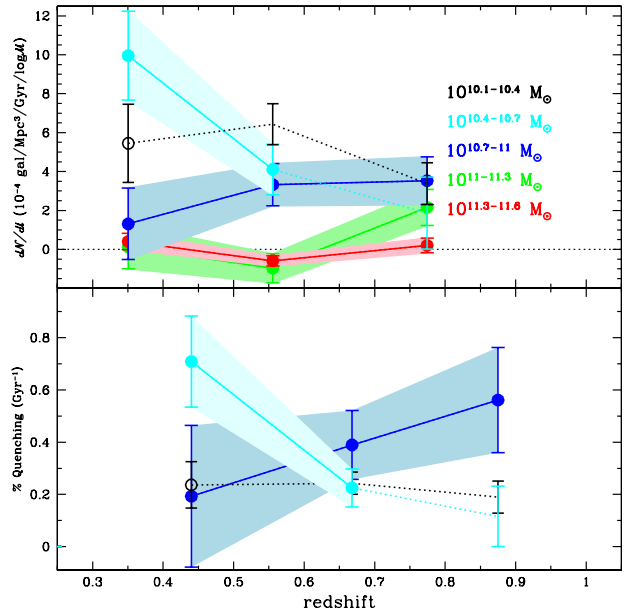


Fig. 16. Evolution of the growth rate in number density $\delta\rho_N/\delta t$ (top panel) as a function of redshift for red galaxies ($PT=1$) in different mass ranges. Values have been plotted at the intermediate redshift between two adjacent redshift bins. In the bottom panel we show the evolution with redshift of the fraction of blue galaxies ($PT=2,3,4$) which are transforming into red galaxies per Gyr (see text). In all the panels hatched regions refer to *GSMF* complete in the mass range and redshift considered, while dotted lines are connecting points at redshifts where the *GSMF* is not complete in the considered mass range.

8.1. The build-up of the red sequence

In this section we try to quantify the growth rate (in number and mass density) of red galaxies as a function of redshift and in different \mathcal{M} ranges. This rate can be interpreted as the flux required for the migration with cosmic time from the blue cloud to the red sequence.

Figure 16 shows the evolution with redshift for the red population ($\mathcal{PT}=1$), in different mass ranges, of the growth rate in number density ($\delta\rho_N/\delta t$, upper panel), estimated using $1/V_{\max}$ data points. For $\log(\mathcal{M}/M_\odot) < 11$ the growth rate is of the order of $10^{-3} - 10^{-4}$ gal/Mpc³/Gyr/log \mathcal{M} and even lower and approaching zero for higher masses. The growth rate in mass density is $\delta\rho_M/\delta t \simeq$ few 10^6 - few 10^7 M_\odot /Mpc³/Gyr/log \mathcal{M} . Integrated above $\log(\mathcal{M}/M_\odot)=9.8$ we find $\delta\rho_N/\delta t=6.8(\pm 1.2) \times 10^{-4}$ gal/Mpc³/Gyr and $\delta\rho_M/\delta t=1.8(\pm 0.4) \times 10^7$ M_\odot /Mpc³/Gyr between the second and the first redshift bin ($z \sim 0.34$). Despite the large errors, we find a clear increase with cosmic time of the growth rate for galaxies with $\log(\mathcal{M}/M_\odot)=10.4-10.7$, while a hint for a decrease with cosmic time at higher \mathcal{M} ($\log(\mathcal{M}/M_\odot)=10.7-11$). These trends can be interpreted as a *mass-assembly downsizing* signal, i.e. most massive red galaxies assembled their mass earlier than lower mass red galaxies. For comparison, in the VVDS Arnouts et al. (2007) find that the median mass growth rate (integrated over the whole mass range $\log(\mathcal{M}/M_\odot)=8-13$) between $z \sim 2$ and $z = 0$ is $1.7(\pm 0.4) \times 10^7$ M_\odot /Mpc³/Gyr, consistent with our values for $\log(\mathcal{M}/M_\odot) > 9.8$. Walcher et al. (2008) derived somewhat higher $\delta\rho_M/\delta t=6.5-10 \times 10^7$ M_\odot /Mpc³/Gyr from $z \sim 1$ to $z \sim 0.5$ integrated over the whole mass range. The difference with our results, indeed, could be due to the more extended mass range.

In principle, this growth rate compared to the number density of blue galaxies should give us an estimate of the fraction of blue galaxies which, at any given time, are transforming into red galaxies (f_Q) due to the quenching of their *SFR*. We have therefore derived the fraction:

$$f_Q(\mathcal{M}) = \frac{(\delta\rho_N/\delta t)^{\text{red}}(\mathcal{M})}{\rho_N^{\text{blue}}(\mathcal{M})} \text{Gyr}^{-1}, \quad (3)$$

using $1/V_{\max}$ estimation for ρ_N . It is shown in the bottom panel of Fig. 16 as a function of redshift and mass. For $\log(\mathcal{M}/M_\odot) > 11$ they are unconstrained, because of the small number density of blue galaxies. The values obtained for $\log(\mathcal{M}/M_\odot) < 11$ range have a median value of $\sim 25\%$ Gyr⁻¹. The fraction of quenching galaxies could be lower, if we consider that the timescale for the transformation into red galaxies could be smaller than 1 Gyr, as suggested by the persistence, at any redshift explored, of the bimodality of the blue and red populations with a small fraction of galaxies in the *green valley*. For example Balogh et al. (2004) estimate in the SDSS a $\Delta t = 0.75$ Gyr if the truncation of the SFH is rapid $\tau < 0.5$ Gyr and we estimate that $\Delta t \simeq \tau$ for $\tau > 1$. As for the growth rate, we find that this fraction decreases with cosmic time for high-mass galaxies, while increases for intermediate mass galaxies at least for $z < 0.7$. At $z < 0.4$ we are not able to explore the blue to red transformation for the low mass regime ($\log(\mathcal{M}/M_\odot) < 10.4$) and to verify whether the trend of the blue fraction to increase with cosmic time for low-mass galaxies is shifted at even lower redshift, as expected in the downsizing scenario. We note however that all fraction val-

ues are still very uncertain and their uncertainties increase further if we include cosmic variance.

Vergani et al. (2009) explore the properties and number densities of the Post-StarBurst (PSB) galaxy population, spectroscopically identified in the zCOSMOS sample, as the possible link population in the transition phase between the blue cloud and the red-sequence. They found that this galaxy population which is affected by a sudden quenching of its star-formation activity, may increase the stellar mass density of the red-sequence by up to a non-negligible level of 10%.

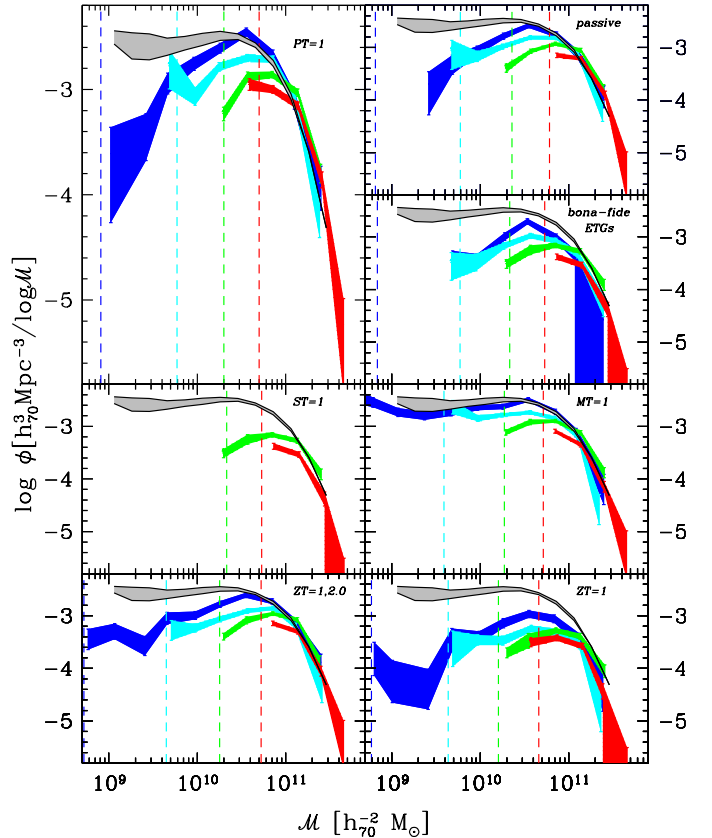


Fig. 17. GSMFs for ETGs using various classification schemes: red galaxies ($\mathcal{PT}=1$), passive ($\log(SSFR/\text{Gyr}^{-1}) < -2$), spheroidals ($ZT=1+2.0$, $ZT=1$, $MT=1$), absorption line galaxies ($ST=1$) and “bona-fide ETGs” as defined in Sec. 4. Only $1/V_{\max}$ determinations have been plotted, with their uncertainties. Different colours refer to different redshift ranges, increasing from blue ($0.10 < z < 0.35$), cyan ($0.35 < z < 0.55$), green ($0.55 < z < 0.75$) to red ($0.75 < z < 1.0$). Grey hatched region refer to local GSMF for ETGs derived from Baldry et al. (2008) and Baldry et al. (2006) (see text).

To derive the fraction above we assume “quenching” as the only effect. One could assume, as opposite extreme case, “major merging” (with mass ratio 1:1 or 1:4) as the only effect, and derive the fraction of galaxies that should merge, to explain the observed growth rate in the red galaxies, using Eq. 2. The fraction of major merging per Gyr among all galaxies is similar to those shown in Figure 8,

since most of the evolution in the global *GSMF* is due to red galaxies. Also if we consider only dry-merging the fraction for $\log(\mathcal{M}/\mathcal{M}_\odot) > 10.6$ is similar (40-10%) and are consistent with the low fraction of the major-merger rate between early type galaxies found by de Ravel et al. (2009) in the VVDS. At low redshifts and masses the fraction of dry-mergers seems to increase but is unconstrained because of the steep decline of the number densities of red galaxies.

8.2. Elliptical/Early type galaxy evolution

Hierarchical semi-analytical models (De Lucia et al. 2006) predict that stars in more massive elliptical galaxies are *older* but assemble their mass through mergers *later* in cosmic time than their lower mass counter-parts. For example, 50% of ellipticals with $\log(\mathcal{M}/\mathcal{M}_\odot) > 11$ form most (80%) of their stars at $z_{\text{form}} \simeq 1.6$, while assemble their mass at $z_{\text{assembly}} \simeq 0.2$, defined as the redshift at which most (80%) of the stars that make up the galaxy at redshift zero are already assembled in one single object. Galaxies with $\log(\mathcal{M}/\mathcal{M}_\odot) > 9.6$, instead, have a median $z_{\text{form}} \simeq 1.3$ and median $z_{\text{assembly}} \simeq 0.9$ (see Fig.4 and 5 in De Lucia et al. 2006). As pointed out by Cimatti et al. (2006), this trend is the opposite of the *mass-assembly downsizing* signal found for red galaxies in the luminosity function, confirmed by Scarlata et al. (2007b), i.e. most massive red galaxies assembled their mass earlier than lower mass red ones. In the following we explore in detail in the zCOSMOS sample the evolution of elliptical and all early type galaxies, using the different classification schemes described in Section 4 and based on colours, morphology, spectral features or a combination of them. In addition, using ZEST morphologies, we further divide ellipticals ($\mathcal{ZT}=1$) from bulge-dominated galaxies ($\mathcal{ZT}=2.0$) and passive galaxies ($\log(SSFR/\text{Gyr}^{-1}) < -2$) from quiescent galaxies ($\log(SSFR/\text{Gyr}^{-1}) < -1$).

Figure 17 shows the evolution as a function of redshift of the *GSMFs* for the different populations of ETGs: red galaxies ($\mathcal{PT}=1$), passive galaxies ($\log(SSFR/\text{Gyr}^{-1}) < -2$), spheroidals ($\mathcal{MT}=1$, $\mathcal{ZT}=1+2.0$, $\mathcal{ZT}=1$), absorption line galaxies ($\mathcal{ST}=1$) and “bona-fide ETGs” as defined in Sec. 4.

First of all we note that significant differences in normalization are present in the *GSMFs* at all \mathcal{M} , with the pure ellipticals classified by ZEST ($\mathcal{ZT}=1$) being the lowest in all redshift and mass ranges explored. On the contrary, the shapes of the various *GSMFs* are all similar, with a steep decline of the number densities for $\mathcal{M} < \mathcal{M}^*$ ($\alpha > -1$) for all *GSMFs*, except for the *GSMF* of the spheroidals with $\mathcal{MT}=1$ which shows an excess at low-mass ($\log(\mathcal{M}/\mathcal{M}_\odot) < 9.5$), in the first redshift bin.

We have studied in more detail this population of low-mass spheroidals ($\mathcal{MT}=1$), which dominates the *GSMF* and presents blue colours ($\mathcal{PT} \geq 2$, i.e. $(U - B)_{\text{rest}} < 1$). We find 89 such objects with $\log(\mathcal{M}/\mathcal{M}_\odot) < 9$ at low redshift ($z < 0.5$). They have quite compact sizes, with a small median effective radius ($r_e \simeq 0.6$ kpc). We find a contribution of blue MRS spheroidals ($\mathcal{PT} \geq 2$, $\mathcal{MT}=1$) also at high mass ($\log(\mathcal{M}/\mathcal{M}_\odot) > 10.5$) at all redshifts (182 objects). This last population of massive blue MRS spheroidals does not dominate the high-mass end of *GSMF* ($\sim 20\%$), as instead does at the low-mass end. Therefore, this suggests that the shape of the *GSMF* of this population of blue spheroidals differs from those of red spheroidals, at least us-

ing MRS morphologies. This is consistent with the study of Zucca et al. (2009) of the contribution of this population to the *B*-band Luminosity Function. However, for these objects, in particular at low-mass, we note that MRS morphologies, do not always agree with ZEST ones, giving an idea of the uncertainties in deriving morphologies for faint low-mass objects. We have, therefore, further checked their morphology visually (by PC, LT, LP). We find that most of blue low-mass MRS spheroidals are bulge dominated spirals (Sa). Most of the massive ones, even if their morphological classifications are in agreement between the two methods (ZEST and MRS), appear to be spirals, from Sa to Sc, although with morphological parameters (asymmetry and concentration) more similar to those of the elliptical class. Composite spectra for this population were generated (following Mignoli et al. 2009) by averaging all their spectra at $z < 0.5$ and dividing them into low-mass and high-mass objects. In Figure 18, the average spectra are plotted: low-mass blue spheroidals show a blue continuum and emission lines typical of star forming galaxies, indicating that these galaxies are undergoing a quite strong star-formation episode, while the high-mass blue spheroidals have on average a red spectrum, with absorption lines, largely indistinguishable from that of the purely passive galaxies (see Mignoli et al. 2009), but with the presence of emission lines which could indicate some nuclear activity contamination (i.e. $[\text{NII}]/\text{H}\alpha$ and $[\text{OIII}]/\text{H}\beta$ consistent with LINERs). The presence of an AGN component could also explain their typical high concentration index obtained from their HST images. The AGN might play a role in quenching the *SFR* in this population of blue elliptical massive galaxies, possibly in the transition phase between the blue cloud and the red-sequence.

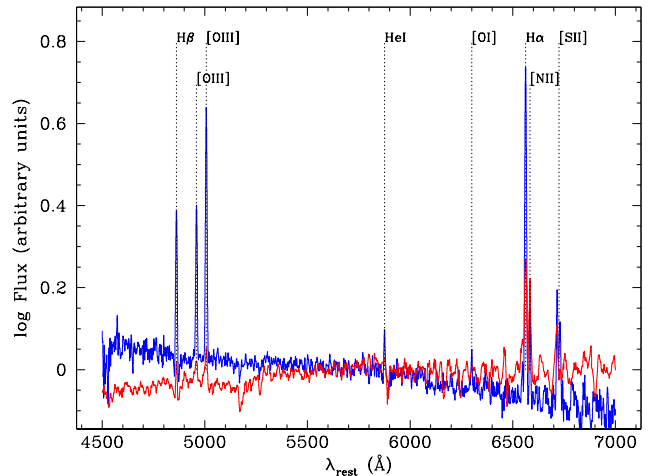


Fig. 18. Stacked spectra for galaxies with MRS elliptical morphology ($\mathcal{MT}=1$) and blue colours ($\mathcal{PT}=2+3+4$) at low-mass ($\log(\mathcal{M}/\mathcal{M}_\odot) < 9$ in blue) and high-mass ($\log(\mathcal{M}/\mathcal{M}_\odot) > 10.5$ in red).

Finally, we have studied the evolution with cosmic time of the *GSMFs* of red, passive, ellipticals, spheroidals, absorption-line and “bona-fide ETG” classes. In Figure 17 we show the *GSMFs* for the various ETGs classes at increasing redshift. We also show, as reference, the local *GSMF* of ETGs. We have derived it using the global *GSMF*

by Baldry et al. (2008) and the fraction of red galaxies estimated by Baldry et al. (2006) for their 4 central environment bins. This is shown in Figure 17 as grey shaded region. We note a very similar evolution for the ETG population using all the different definitions to classify an ETG. As claimed for red galaxies, we find a clear “mass-assembly downsizing” evolution, with no evidence for an increase with cosmic time in the number density of the most massive ETGs since $z \sim 1$ and a progressive increase of the *GSMF*s at intermediate mass ($\log(\mathcal{M}/\mathcal{M}_\odot) < 11$) out to $z = 0$. We find that also using M05 models to estimate the stellar masses the same trend is visible in our data, not affecting strongly our main conclusions. This is due to the fact that in the redshift range sampled here ($0.1 < z < 1.0$) ETGs have on average old stellar populations not dominated by TP-AGB in particular for massive objects.

Similar results for massive ETGs have been firstly noted in the near-IR (*K*-band) Luminosity Function by Pozzetti et al. (2003) and in the Mass Function by Fontana et al. (2004) in the K20 survey, using spectral classification, and confirmed more recently by larger optical and near-IR surveys such as the VVDS using colours or spectra to define ETGs (Zucca et al. 2007, Arnouts et al. 2007, Vergani et al. 2008). Scarlata et al. (2007b) found that in COSMOS both the morphologically and the photometrically selected subsamples of ETGs show no evolution in the number density at the bright-end of B-band Luminosity Function ($L > 2.5L^*$) out to $z \sim 0.7$, and a deficit of a factor of about 2–3 of fainter ETGs over the same cosmic period, also confirmed by Zucca et al. (2009) in the zCOSMOS sample. Ilbert et al. (2009), selecting ETGs (by morphology or colour) in SCOSMOS (Sanders et al. 2007) with accurate photometric redshift (Ilbert et al. 2009) up to $z_{\text{photo}} = 2$, found similar results for massive ETGs at $z < 1$ (evolution < 0.2 dex for $\log(\mathcal{M}/\mathcal{M}_\odot) > 11$) and a faster evolution at higher redshifts (by a factor 15–20 between $z = 1.5 - 2$ and $z = 0.8 - 1$) or smaller masses (increasing by a factor 4.5 between $z = 0.8 - 1$ and $z = 0.2 - 0.4$ for $\log(\mathcal{M}/\mathcal{M}_\odot) \sim 10$).

8.3. The building redshift of ETGs

This result suggests that lower mass ETGs (regardless of the method used to classify them) assembled their mass later than high-mass ETGs. We can estimate, indeed, the redshift at which 50% of ETGs have been already build-up (z_{building}), as a function of their stellar mass, i.e. at which redshift their number density has decreased by a factor 2 from $z = 0$. This definition is similar to the median z_{assembly} in De Lucia et al. (2006) if we assume only a small increase (at most by a factor 2) in stellar mass due to merging down to $z = 0$. This assumption seems to be reasonable given the observed mild evolution of the high-mass end of the *GSMF* since $z \sim 1$. For example, assuming a significant increase (due to 5 events of major-merging) in stellar mass of about half of the ETGs (dry-mergers) or of the global (wet+dry mergers) population at $\log(\mathcal{M}/\mathcal{M}_\odot) \sim 10.3$ from $z = 0.5$ to $z = 0$, the number density of ETGs with $\log(\mathcal{M}/\mathcal{M}_\odot) \sim 11$ should increase by more than 25–30%, which is not observed. A higher number of progenitors for the most massive ellipticals is not even predicted by semi-analytical models (reaching up to ~ 5 progenitors for $\log(\mathcal{M}/\mathcal{M}_\odot) \sim 11$ and even less for lower mass galaxies in De Lucia et al. 2006). Since we are sampling the number densities of ETGs only above $z > 0.25$, we

are able to derive only upper limits to z_{building} , as defined above, at least in the low mass range. For this reason we have used as local reference the *GSMF* for ETGs, described above and shown in Figure 17 as grey shaded region.

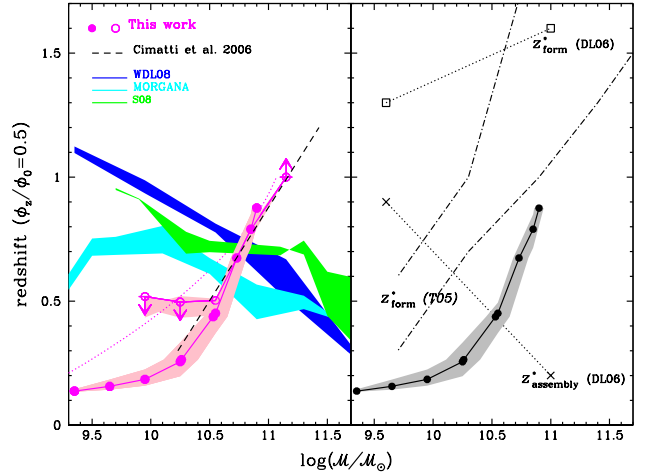


Fig. 19. Redshift at which ETGs *GSMF* has decreased by a factor 2 ($\phi_z/\phi_0 = 0.5$, i.e. z_{building} , see text) as a function of \mathcal{M} . *Left panel:* Magenta points refer to data derived within zCOSMOS for passive galaxies ($\log(SSFR/\text{Gyr}^{-1}) < -2$). Open circles have been derived completely from zCOSMOS dataset, using as reference the *GSMF* in the first redshift bin ($\phi_0 = \phi(z \sim 0.24)$, along with the region covered using various ETGs classification criteria. Filled points are z_{building} using the local ETGs *GSMF* (see text), along with the uncertainties in its shape due to environment and or ETGs classification criteria. Dotted magenta curve shows the \mathcal{M}_{min} above which we are formally complete. Also plotted z_{building} from SAM: WDL08 (in blue), S08 (in green) and MORGANA (in cyan), derived using the original *GSMF* or convolved with 0.25 dex in mass uncertainties (see Fontanot et al. 2009). *Right panel:* z_{building} for zCOSMOS data points are compared with the trend with stellar mass of the median z_{assembly} and z_{form} from De Lucia et al. (2006, DL06) and with the redshift at which ends up the stellar formation in local ETGs estimated by Thomas et al (2005, T05) in different environments.

Within the zCOSMOS redshift range we find for ETGs galaxies a z_{building} increasing with \mathcal{M} regardless of classification method, with $z_{\text{building}} \sim 0.4, 0.5, 0.8$ for $\log(\mathcal{M}/\mathcal{M}_\odot) \sim 10, 10.4, 10.8$, respectively (Figure 19). At higher mass the number density of ETGs is almost constant up to redshift ~ 0.7 , and decreases by less than a factor of 2 since $z \sim 1$, therefore we conclude that $z_{\text{building}} > 1$ for $\log(\mathcal{M}/\mathcal{M}_\odot) > 11$. Our estimates of z_{building} for passive galaxies ($\log(SSFR/\text{Gyr}^{-1}) < -2$) are shown in Fig. 19, derived within the redshift range explored in zCOSMOS (open circles), along with the region covered by the different classification criteria. Since the local ETGs *GSMF* derived from Baldry et al. (2006, 2008) as described previously, approaches the observed zCOSMOS *GSMF* in the first redshift bin for $\log(\mathcal{M}/\mathcal{M}_\odot) > 10.5$ for passive galaxies, z_{building} should be considered upper limit only below this mass. Most of the points have $\mathcal{M} > \mathcal{M}_{\text{min}}$, above which we are formally complete. We also show z_{building} assuming

the local *GSMF* for ETGs. We note that the exact z_{building} values at low masses could be affected by different classification method between local and high- z ETGs, for these reason we show also the region covered using the different fractions of ETGs in all the environment bins in Baldry et al. (2006), which could mimic the variation with the classification method of the local ETGs *GSMF*'s. First of all we note that the “downsizing” trend with mass in ETGs z_{building} is clearly visible. Our data are in very good agreement with values derived by Cimatti et al. (2006), who have used the de-evolved luminosity function for galaxies in the red-sequence. The values of z_{building} are quite in agreement with the end of the star formation histories estimated by Thomas et al. (2005) for early-type galaxies as a function of stellar mass from their spectral properties, in particular for the low density environments (T05, in the right panel of Fig. 19). This downsizing trend with stellar mass is instead in contrast with semi-analytical predictions for z_{assembly} (e.g. by De Lucia et al. 2006, DL06, shown in the right panel of Fig. 19).

For a more appropriate comparison with semi-analytical models (SAM) we use z_{building} derived with exactly the same definition used for the data. We use the predictions of the *GSMF* for the three prescriptions used in Fontanot et al. (2009): the most recent implementation of the Munich SAM (De Lucia & Blaizot 2007, Wang et al. 2008a, hereafter WDL08), the MORGANA model (Monaco et al. 2007, Lo Faro et al. 2009), and the fiducial model presented by Somerville (2008, hereafter S08). We have used the same classification criteria for passive galaxies ($\log(SSFR/\text{Gyr}^{-1}) < -2$) used in the models. The predicted *GSMF*'s for each model are shown in Fig. 6 in Fontanot et al. (2009). In Figure 19 we have compared z_{building} derived from *GSMF* SAM predictions (provided us by Fontanot) and zCOSMOS data using exactly the same definition. For each models we show the region covered by z_{building} using the original SAM *GSMF*'s and those which take into account 0.25 dex of uncertainties in mass derivation. Opposite to the data, the semi-analytical models show a reverse trend with mass of z_{building} similar to the trend of z_{assembly} due to the relevance of merging processes and opposite to the trend with mass in the redshift at which stars form (z_{form} , see Fig. 19 right panel). Residual small differences for example in the determination of the mass or SFR in the data respect to the models (e.g. the presence of secondary bursts in model SFH) or in the ETGs classification criteria are unlikely able to reconcile the opposite trend with mass.

These results argue against a dominant contribution of mergers at $z < 1$ in building up ETGs galaxies, or in any case against an increasing contribution of mergers with mass, as predicted by semi-analytical models (see Fig. 2 in Wang & Kauffmann 2008). We conclude therefore that the build-up of ETGs galaxies follows the same “downsizing” trend with mass of the formation of their stars, opposite to the “upsizing” trend in SAMs. The increase in number density of intermediate mass ETGs can be explained with a conversion of blue, irregular, and disk galaxies into “red” ETGs, not excluding, even if not dominant, also gas-rich mergers.

8.4. Timescales for the quenching of the star formation and morphological transformation

The evolution with redshift in the number densities in different mass ranges for three different samples of ETGs (red ($\mathcal{PT}=1$), spheroidal ($\mathcal{ZT}=1,2,0$) and quiescent ($\log(SSFR/\text{Gyr}^{-1}) < -1$) galaxies) is shown in Figure 20. We find that they all show a very similar trend (but different normalization), with an increase of the number densities of intermediate mass ETGs with cosmic time from $z = 1$ towards the local Universe. This trend is steep for low-intermediate mass galaxies and is flat and almost negligible only for $\log(\mathcal{M}/\mathcal{M}_{\odot}) > 11$ (< 0.1 dex between $z = 0.85$ and $z = 0.25$ for $\log(\mathcal{M}/\mathcal{M}_{\odot})=11-11.5$). An evolution similar for red and spheroidal galaxies has been already noted by Arnouts et al. (2007), who commented: “If not by chance, this coincidence could suggest that the build-up of the quiescent sequence is closely followed or preceded by a morphological transformation.” In principle, if all the various classification methods here adopted were “perfect”, the fact that the number density of SED-ETGs is higher than that of the morpho-ETGs, at a given mass, would suggest that the colour transformation (from blue to red) precedes or have a shorter time scale of the morphological transformation. From Fig. 20 the delay time between the colour and the morphological transformation could be estimated, at a fix ρ_N , to be about 1-2 Gyr (shown as an arrow for $\log(\mathcal{M}/\mathcal{M}_{\odot})=10.7-11$). In addition, since the number density of the low-*SSFR* population is higher than that of the red galaxies (SED-ETGs), we can estimate that the time elapsed for quiescent galaxies to completely switch off the SFR and become red is of the same time-scale (about 1-2 Gyr, shown as an arrow in Fig. 20). Wolf et al. (2008) reach a similar conclusion in the cluster A901/2 at $z \sim 0.17$: the rich red spiral population at intermediate mass ($\log(\mathcal{M}/\mathcal{M}_{\odot}) = [10, 11]$) is best explained if quenching is a slow process and morphological transformation is delayed even more (see also Skibba et al. 2008). The small contribution to the assembly of the red-sequence by the class of post-starburst galaxies (most of which are assumed to fast quenching of their star formation) further supports this scenario of delayed/slow quenching (Vergani et al. 2009).

However, we are aware that the colour selected red galaxies could be contaminated by dusty starburst. We remind here that, given the $24 \mu\text{m}$ flux limit of ~ 0.3 mJy, only 5% of red galaxies (SED-ETGs) have been detected at $24 \mu\text{m}$ (all having $\log(SSFR/\text{Gyr}^{-1}) > -2$), and about 23% have $-2 < \log(SSFR/\text{Gyr}^{-1}) < -1$, i.e. they are not completely “dead”. On the other hand also among elliptical galaxies exist a non-negligible blue population ($\sim 20\%$), for which therefore the morphological transformation could precede or is faster than the colour transformation (see below for a discussion). Therefore, we have checked that also the number density of red passive galaxies ($\mathcal{PT}=1$ and $\log(SSFR/\text{Gyr}^{-1}) < -2$), i.e. “red & dead”, is higher at any given mass and redshift than the number density of passive elliptical galaxies ($\mathcal{ZT}=1,2,0$ and $\log(SSFR/\text{Gyr}^{-1}) < -2$), and at a given number density and mass they are delayed by 1-2 Gyr. We can conclude that, at least statistically, the morphological transformation takes longer time than for the galaxy to become “red and dead”.

But which physical processes induce these transformations? *SSFR*, colours or photometric types depend on the

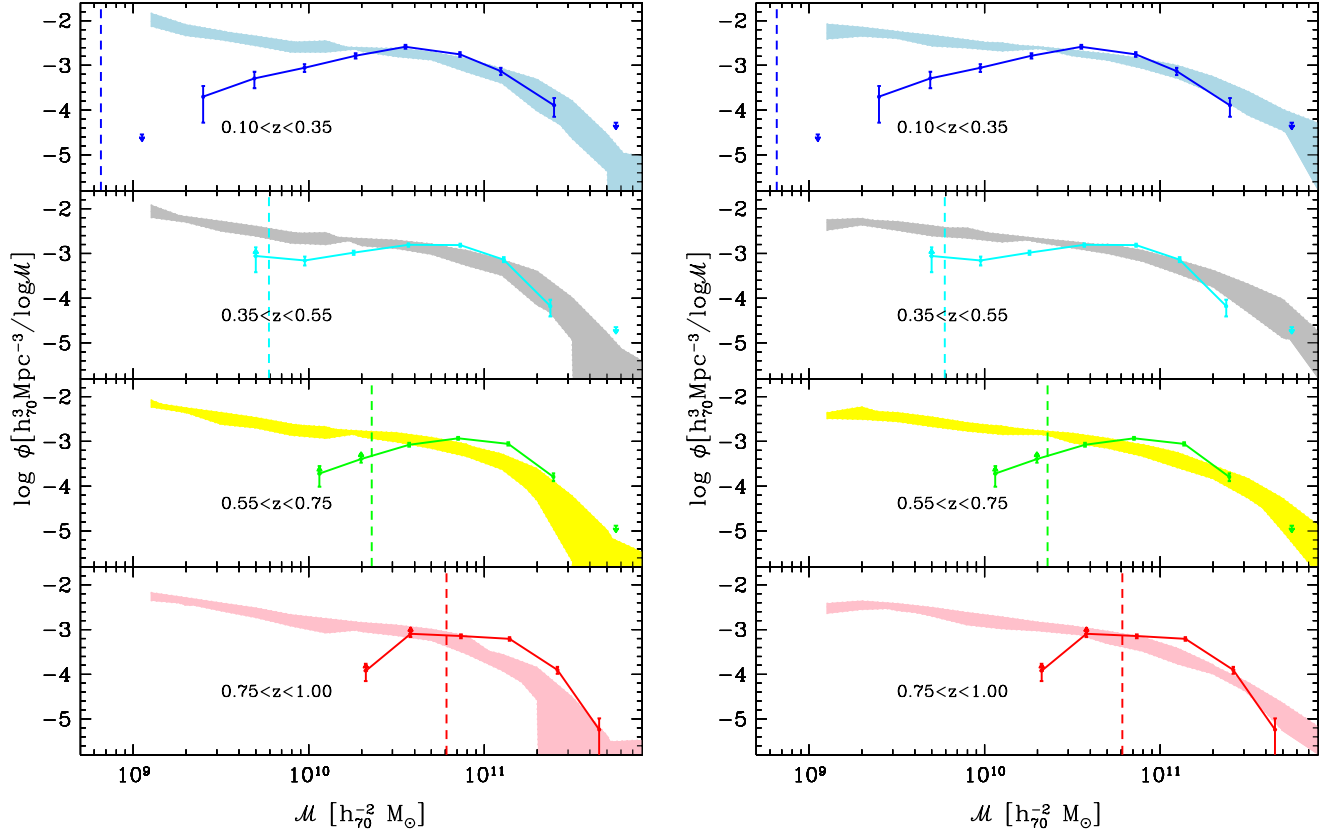


Fig. 21. Comparison between observed *GSMFs* (lines and points) with the regions covered by the predictions (shaded colour regions) of three semi-analytical models (Morgana, WDL08 and S08 from Fontanot et al. 2009), at increasing redshifts (from top to bottom panels). *Left panels:* original *GSMFs* from SAM. *Right panels:* SAM *GSMFs* take into account 0.25 dex of uncertainties in the \mathcal{M} derivation.

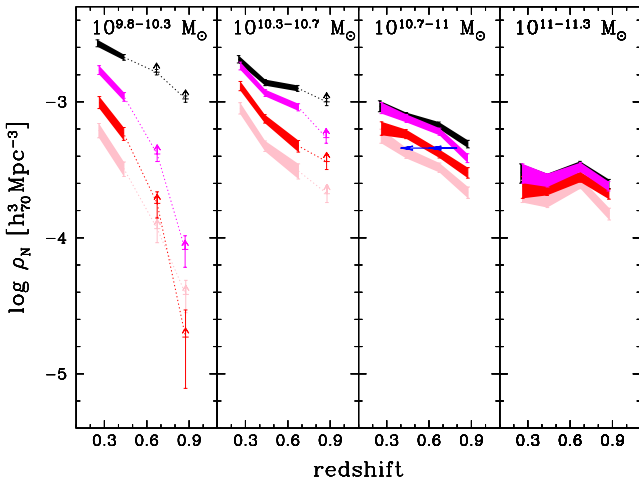


Fig. 20. Number density evolution for ETGs in different mass ranges: red galaxies (red for $\mathcal{PT}=1$), spheroidals (pink for $\mathcal{ZT}=1+2.0$) and low-*SSFR* (magenta for $\log(\mathit{SSFR}) < -1$). Black regions and symbols are for the global population. Symbols and lines have the same meaning as in Figure 12. In the 3rd panel we also indicate by 2 arrows the evolutionary time sequence from quiescent to red to spheroidal galaxies (see text).

star formation history, while morphological types mainly reflect the dynamical history of a galaxy. The transformation from active blue galaxies into red passive galaxies, as well as the transformation from spiral disc-dominated to bulge-dominated systems, could be driven by a variety of processes such as the aging of their stellar population or the fading of the disc, due to the exhaustion of gas reservoir, or to the gas stripping, or to the quenching of the SFHs, for example by the AGN feedback (Menci et al. 2006, Monaco et al. 2007, Bower et al. 2006), or by truncating the gas accretion from infall or from satellite galaxies. Also “starvation” (or “strangulation”) is expected to affect a galaxy star formation history on a quite long timescale and therefore to cause a slow declining activity: when a galaxy is accreted onto a larger structure, the gas supply can no longer be replenished by cooling that is suppressed (Larson et al. 1980). This process represents one important element of semi-analytic models of galaxy formation. Some of the processes mentioned above are obviously environment dependent.

On the other hand, the strong increase of intermediate mass pure morphological ellipticals ($\mathcal{ZT}=1$) or “bona-fide ETGs” (red passive spheroidals) argues for dynamical processes, such as the merging between two low mass galaxies (Toomre & Toomre 1972, Barnes 1992). Mergers are included in standard semi-analytic models of galaxy formation and represent indeed the main channel for the forma-

tion of bulges. Menci et al. (2002) included into hierarchical semi-analytical models also binary aggregations of satellite galaxies inside a common halo. However, if merger events are responsible for the morphological transformation, we should expect a rapid evolution from blue to red after the formation of the bulge/elliptical, i.e. after the burst triggered by the merger (Mihos & Hernquist 1996). We find, instead, that the colour transformation precedes the morphological one, and that only a population ($\sim 20\%$) of massive blue spheroidal exist, which could be the end-product of a merger events. The massive tail of this population has some signature of an AGN component in its stacked spectrum (see Fig. 18), which could be the responsible of the quenching of the SFR , allowing their transition into red elliptical with cosmic time. The study of this particular population is beyond the aim of this paper and it will be the subject of future zCOSMOS papers.

Our results, therefore, suggest different dynamical processes as the main mechanism for the morphological transformation after the colour transformation. For example, bulge growth through disc instability could be efficient (Carollo et al. 2001, Bower et al. 2006, Dekel et al. 2009). Disc instability is also included as a channel for the formation of the bulges in the SAMs (De Lucia et al. 2006, Bower et al. 2006, Parry et al. 2009). Recently, also dynamical observations of massive galaxies at $z \simeq 2$ with SINFONI (Genzel et al. 2006, 2008) suggest disc instability to build up massive bulges, even without major mergers. Indeed, the dynamical friction and viscous processes at $z \simeq 2$ proceed on a timescale of < 1 Gyr, at least one order of magnitude faster than in $z \sim 0$ disc galaxies. In overdense environments, such as clusters, also the ram pressure could play a role, tearing away the star forming disc (Cortese et al. 2006).

9. Comparison with models

To address the origin of the “age-downsizing” of elliptical galaxies, according to which the stars in more massive galaxies formed earlier and over a shorter period than those in less massive galaxies, Cattaneo et al. (2008) discuss a model in which the star formation is shutdown in dark matter haloes above a critical mass of $\sim 10^{12} \mathcal{M}_\odot$. However, such a model predicts an evolution in the massive tail of the $GSMF$ of red galaxies faster than that at the intermediate-mass from $z = 1$ to $z = 0$, which is in contrast, at least qualitatively, with our results (see Ilbert et al. 2009 for a comparison between model and data).

The same behaviour is clearly visible in Figure 6 in Fontanot et al. (2009) which shows that the evolution of the $GSMF$ for passive galaxies with redshift follows exactly the opposite trend with mass and cosmic time observed in the data (compare with our Figure 17). They also conclude that a robust prediction of SAM models seems to be that the evolution of less massive galaxies is slower and later of that of more massive ones, i.e. the models do not predict “mass-downsizing” but rather the opposite behaviour (sometimes called “upsizing”). Here we recall that the three semi-analytical model renditions in Fontanot et al. (2009) are indeed not able to reproduce the “mass-assembly downsizing” evolution of the observed ETGs $GSMF$, as parametrized for example with the median building redshift described in the previous section (Fig. 19).

In Figure 21 we show also the direct comparison of zCOSMOS ETGs $GSMF$ with the SAM model predictions

for passive galaxies ($\log(SSFR/\text{Gyr}^{-1}) < -1$). Hatched region show the range covered by the three models from Fontanot et al. (2009) for the original $GSMFs$ (left panel) and convolved with 0.25 dex uncertainties in the mass estimate (right panel). A more detailed and quantitative comparison between each model and data is beyond the aim of this paper. We first note that the shape of predicted $GSMFs$ is different from that of the observed $GSMFs$ in all mass and redshift range explored. In particular models are not able to recover the steep decline with decreasing mass of the number densities of passive ETGs, overproducing their number densities with decreasing mass, overproducing their number densities for $\log(\mathcal{M}/\mathcal{M}_\odot) < 10.3$. This is due to the fact that in the models intermediate mass galaxies formed too early and are too passive and red at late times. On the contrary at the massive end ($\log(\mathcal{M}/\mathcal{M}_\odot) > 11$) the original models have the well-known problem to underestimate massive galaxies at high redshift (for $z > 0.6$ in zCOSMOS dataset). We show that the convolution with stellar mass uncertainties (0.25 dex) only partially solve the problem at high-redshift and masses ($\log(\mathcal{M}/\mathcal{M}_\odot) > 11.3$), while models continue to underpredict $GSMFs$ around $\log(\mathcal{M}/\mathcal{M}_\odot) \sim 11 - 11.3$, not reproducing the $GSMFs$ shape, and they start to overproduce massive galaxies at low redshifts, as already pointed out by Fontanot et al. (2009). To qualitatively reconcile data and models at the massive-end, the mass uncertainties should increase rapidly with redshift, which is not the case for most of current surveys with accurate and multi-band photometry extended to near-IR rest-frame wavelength.

We conclude that the three semi-analytical model explored here (WDL08, MORGANA and S08) are not able to completely reproduce either the observed shape of the $GSMFs$ of passive galaxies either the evolutionary trend. In particular SAMs overpredict the low-mass ETGs number densities and, even if the uncertainties in \mathcal{M} determination partially solve the underprediction at high masses and redshifts, they predict an evolution with cosmic time with an opposite trend with mass to what observed in the data, i.e. they are not able to reproduce the later and faster evolution in number densities at lower masses (“mass-assembly downsizing”).

10. Summary and conclusions

We have investigated the evolution of the Galaxy Stellar Mass Function up to to $z = 1$ using the zCOSMOS 10k bright spectroscopic survey using VIMOS (~ 8500 galaxies with $15.0 < I < 22.5$ over 1.4 deg^2) and multiband photometry (from UV to near-IR). The main observational results can be summarized as follows:

- *Unveiling bimodality in the GSMF*: The shape of the $GSMF$ is better reproduced by two Schechter functions at least up to $z \simeq 0.55$, the maximum redshift at which we can explore the $GSMF$ upturn due to our mass limit. This shape is linked to the bimodality in galaxy properties of ETGs/LTGs populations, which dominate respectively the $GSMF$ at high-masses ($\log(\mathcal{M}/\mathcal{M}_\odot) > 10.5$) and at low/intermediate-masses up to the highest redshift explored ($z \simeq 1$).
- *Mass-Assembly Downsizing*: We find a continuous and faster rising with cosmic time from $z \simeq 1$ down to $z = 0$ of the global $GSMF$ for $\log(\mathcal{M}/\mathcal{M}_\odot) < 11$ (a factor

~ 2 for $\log(\mathcal{M}/M_{\odot}) \sim 10.5$) and a more slow increase ($< 15\%$) for $\log(\mathcal{M}/M_{\odot}) > 11$. A similar trend is even stronger for the ETGs population, i.e. massive galaxies build-up their stars and mass earlier than lower mass galaxies. We show that the z_{building} for ETGs increases rapidly with \mathcal{M} with $z \sim 0.2 - 0.8$ for $\log(\mathcal{M}/M_{\odot}) = 10 - 10.8$ and is significantly higher ($z \gtrsim 1$) for massive ETGs.

- “*SFHs evolved GSMF*” and mergers: Assuming only a growth in stellar mass driven by exponentially decreasing star formation histories, we find that the predicted “*SFHs evolved GSMFs*” agree with the observed *GSMF*s with differences at most of 20-40%, even if they predict somewhat too red colours than observed, in particular at low redshift. Mass assembly driven by SFH can explain most of the evolution at intermediate-low \mathcal{M} ($\log(\mathcal{M}/M_{\odot}) < 10.6$). The low/negligible evolution at higher \mathcal{M} sets a limit of 30-10%, decreasing with redshift, to the fraction of major merging among the global galaxy population. Major merging events are, if not marginal, not dominant in the evolution processes.
- $\mathcal{M}_{\text{cross}}$: The intersection ($\mathcal{M}_{\text{cross}}$) of the *GSMF*s of the ETG/LTG populations decreases with cosmic time. This is due mainly to a clear increase with cosmic time of the number density of ETGs, regardless of their classification method, with $\log(\mathcal{M}/M_{\odot}) < 11$. For LTGs, instead, the number density of blue or disc+irregular galaxies shows only a mild or negligible evolution, while the most extreme population of star forming galaxies (the ones with high specific star formation) is decreasing fast in number density with cosmic time, in particular at high masses ($\log(\mathcal{M}/M_{\odot}) > 10.3$).
- *Flow to build-up the red population*: We have derived the flow from blue to red population at different redshifts and masses. We find a growth rate in number and mass density of the red galaxies of about few 10^{-4} gal/Mpc³/Gyr/log \mathcal{M} and few $10^6 - 10^7$ M_{\odot} /Mpc³/Gyr/log \mathcal{M} for $\log(\mathcal{M}/M_{\odot}) < 11$, and lower above this mass. The corresponding fraction of blue galaxies which, at any given time, are transforming into red per Gyr is on average $\sim 25\%$ for $\log(\mathcal{M}/M_{\odot}) < 11$. This fraction and the growth rate for red galaxies increase with cosmic time at $\log(\mathcal{M}/M_{\odot}) = 10.4 - 10.7$ at least for $z < 0.7$, while it seems to decrease with cosmic time at higher \mathcal{M} ($\log(\mathcal{M}/M_{\odot}) = 10.7 - 11$).
- *ETGs evolution sequence*: Using different methods to classify ETGs, we find that the number density of quiescent galaxies is higher than that of red galaxies, which is even higher than that of spheroidals for $\log(\mathcal{M}/M_{\odot}) < 11$. This behaviour suggests a transformation from quiescent to red objects, mainly due to SFHs, before or on a shorter timescales than the morphological transformation, mainly driven by dynamical processes.
- *Comparison with SAM*: Semi-analytical models are not able to fully account for *GSMF* evolution, in particular for ETGs. They show a different shape at any mass and redshift explored, with a strong excess of low mass passive galaxies and defect of high-mass galaxies at high- z , only partially solved by the bias introduced by uncertainties in the mass determination. Furthermore they predict an “upsizing” evolution in number density with cosmic time, i.e. slower and earlier in low-mass galaxies, opposite to the “downsizing” observed in zCOSMOS data for the *GSMF* and quantified by z_{building} .

Here we try to summarise our results within a galaxy evolutionary scenario which emerges from several observational studies. In particular it is almost established an age-downsizing context for the galaxy stellar populations, according to which less massive galaxies contain younger stars, valid also within the same spectral/morphological types, both in the ETG one (Nelán et al. 2005; Thomas et al. 2005; Graves et al. 2007, Fontana et al. 2004) and in the LTG one (Noeske et al. 2007a,b). We find, furthermore, that downsizing is also valid for the mass-assembly, i.e. massive galaxies have assembled their mass in a single object earlier than low-mass galaxies, both for the global population and for ETGs, regardless of their definition (in colours, in morphology or in the SFR activity). There is, therefore, the possibility that the bimodality properties are a direct consequence of downsizing evolution of galaxies.

We suggest, therefore, a scenario where intermediate-mass galaxies ($\log(\mathcal{M}/M_{\odot}) = 10 - 11$) decrease their star formation activity to intermediate-activity gradually (with an e-folding time $\tau = 1 - 3$ Gyr) and finally to quiescent galaxies, through the exhaustion of the gas reservoir or cold gas accretion or the quenching due to AGN feedback. Noeske et al. (2007a,b) found that the e-folding time is mass dependent, being longer for less massive galaxies, which have also a later onset of the SFH. Therefore, if no other mechanism intervenes to switch on again the star formation activity (re-juvenation hypothesis, Hasinger et al. 2008), they evolve to red colours in a time scale of 1-2 Gyr and finally they undergo a dynamical morphological transformation into spheroidal galaxies.

Since ETGs and in general massive ($\log(\mathcal{M}/M_{\odot}) > 11$) galaxies are already in place at $z = 1$, and their *GSMF* show a negligible evolution after, we conclude that mergers (dry and wet) events are inefficient ($\sim 15\%$ per $\log(\mathcal{M}/M_{\odot}) > 11$) to form the most massive ETGs below $z \sim 1$. The density of intermediate-mass ETGs instead continues to increase with cosmic time (by a factor $\sim 4 - 2$ from $z = 0.7$ to $z = 0.2$ for $\log(\mathcal{M}/M_{\odot}) = 10.3 - 10.7$) with a growth rate of few 10^{-4} gal/Mpc³/Gyr/log \mathcal{M} and few 10^{-7} M_{\odot} /Mpc³/Gyr/log \mathcal{M} . We find that the most efficient evolutionary process to explain our results is the transformation from blue to red galaxies through the smooth decrease or the quenching of the SFR (as described above), followed by a morphological transformation likely through internal dynamical processes, such as disc instabilities. Merger events unlikely can justify the fact that colour transformation precedes the morphological one and in any case they do not dominate ($< 30\%$ in mass growth) at intermediate-high masses ($\log(\mathcal{M}/M_{\odot}) > 10$). Conversely, blue galaxies at low-mass ($\log(\mathcal{M}/M_{\odot}) < 10$) continue to grow in stellar mass, due to their high-SSFR, and replace intermediate-mass LTGs whose density remains almost constant in time. Indeed we find that only a small fraction of low-mass ($\log(\mathcal{M}/M_{\odot}) \sim 10$) blue galaxies is necessary to be transformed into red galaxies to explain ETGs growth rate at least at $z \geq 0.4$. A fraction of them could undergo a wet-merger event to build-up intermediate mass ETGs galaxies at $z < 1$.

Following a schematic diagram, as originally used by Faber et al. (2007), this scenario is presented in Figure 22. The dominant processes are the transformation with cosmic time of blue star forming galaxies of progressively lower mass into red passive galaxies following their SFH. Different evolutionary tracks are plotted between 0.1

and 10 Gyr and refer to SFHs with different timescales (longer for less massive galaxies) and normalized to the total final mass (\mathcal{M}_{tot}). We show, as examples only qualitatively reproducing our data, tracks for models with $(\tau; \log(\mathcal{M}_{\text{tot}}/\mathcal{M}_{\odot})) = (0.1; 11.5)$, $(0.3; 11.0)$ [red curves]; $(0.6; 10.7)$, $(1; 10.3)$, $(2; 10.0)$ [green curves]; $(5; 11)$, $(10; 10)$, $(15; 9)$ [blue curves].

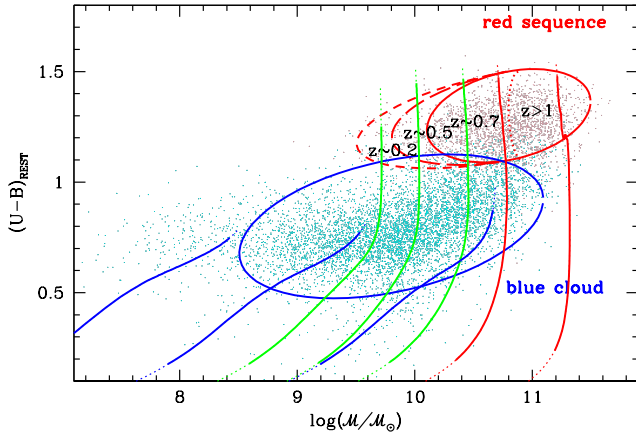


Fig. 22. Schematic scenario for galaxy evolution. Different ellipses refer to different redshifts, while different evolutionary tracks are plotted between 0.1 and 10 Gyr and refer to SFHs with different timescales and normalized to the total final mass $((\tau; \log(\mathcal{M}_{\text{tot}}/\mathcal{M}_{\odot})) = (0.1; 11.5)$, $(0.3; 11.0)$ [red curves]; $(0.6; 10.7)$, $(1; 10.3)$, $(2; 10.0)$ [green curves]; $(5; 11)$, $(10; 10)$, $(15; 9)$ [blue curves].

We conclude that the build-up of galaxies, and ETGs in particular, follows the same “downsizing” trend with mass (i.e. earlier in high-mass galaxies) of the formation of their stars and opposite to that predicted by current SAM models. The galaxy formation and evolutionary scenario is therefore changing towards one in which a smoother evolution in mass growth and star-formation (due to accretion of cold gas) plays an important role compared to major merging events. Major mergings are not marginal but their frequency ($< 30\%$) seems to decrease with redshift and to be constant or decreasing with mass for high-mass galaxies, at odd to SAM models (Wang & Kauffmann 2008). In this scenario, however, it appears quite difficult to explain the “fine-tuning” of the transformation of low-mass into intermediate-mass blue galaxies which is required to maintain their number density approximately constant at any given mass. We expect in such scenario a negligible evolution of the Galaxy Baryonic Mass Function (*GBMF*) for the global population at all masses and a decrease with cosmic time of the *GBMF* for the blue galaxy population at intermediate-high masses.

Acknowledgements. LP wish to thank Fabio Fontanot and Gabriella De Lucia for the stimulating discussions and to have provided SAM models and derived properties in electronic form. We acknowledge support from an INAF contract PRIN-2007/1.06.10.08 and an ASI grant ASI/COFIS/WP3110 I/026/07/0.

References

Abraham, R. G.; van den Bergh, S.; Nair, P., 2003, ApJ, 588, 218

- Arnouts, S., Walcher, C. J., Le Fèvre, O., et al. 2007, 476, 137
 Baldry, I.K., Glazebrook, K., Brinkmann, J., et al. 2004, ApJ, 600, 681
 Baldry, I.K., Balogh, M. L., Bower, R. G., et al. 2006, MNRAS, 373, 469
 Baldry, I.K., Glazebrook, K., Driver, S. P., et al. 2008, MNRAS, 388, 945
 Balogh, M. L.; Baldry, I. K.; Nichol, R.; et al. 2004, ApJ, 615, L101
 Barnes, J. E. 1992, ApJ, 393, 484
 Bauer, A. E., Drory, N., Hill, G. J., Feulner, G., et al. 2005, ApJ, 621, L89
 Bell, E. F., McIntosh, D. H., Katz, N., & Weinberg, M. D. 2003, ApJ, 149, 289
 Bell, E. F., Wolf, C., Meisenheimer, K., et al. 2004, ApJ, 608, 752
 Bell, E.F., Phleps, S., Somerville, R. S., et al. 2006, ApJ, 652, 270
 Bell, E. F.; Zheng, X. Z.; Papovich, C.; et al. 2007, ApJ, 663, 834
 Bertoldi, F., Carilli, C., Aravena, M., Schinnerer, E., et al. 2007, ApJS, 172, 132
 Blanton, M.R., Hogg, D.W., Bahcall, N.A. et al. 2003, ApJ, 594, 186
 Blanton, M. R.; Lupton, R. H.; Schlegel, D. J.; et al., 2005, ApJ, 631, 208
 Bolzonella, M., Miralles, J.-M., Pelló, R. 2000, A&A, 363, 476
 Bolzonella, M., Kovač, K., Pozzetti, L. et al. 2009, A&A submitted (arXiv:0907.0013)
 Brinchmann, J., Ellis, R. S. 2000, ApJ, 536, L77
 Brinchmann, J., Charlot, S., White, S. D. M., et al. 2004, MNRAS, 351, 1151
 Bruzual, G., & Charlot, S. 2003, MNRAS, 344, 1000
 Bundy, K., Ellis, R.S., Conselice, C.J., et al. 2006, ApJ, 651, 120
 Borch, A., Meisenheimer, K., Bell, E. F., et al. 2006, A&A, 453, 869
 Bower, R. G., Benson, A. J., Malbon, R., et al. 2006, MNRAS, 370, 645
 Calzetti, D., Armus, L., Bohlin, R. C., et al. 2000, ApJ, 533, 682
 Capak, P., Aussel, H., Ajiki, M., et al. 2007, ApJS, 172, 99
 Caputi, K. I., McLure, R. J., Dunlop, J. S., et al. 2006, MNRAS, 366, 699Q
 Carollo, C. M.; Stiavelli, M.; de Zeeuw, P. T.; Seigar, M.; Dejonghe, H., 2001, ApJ, 546, 216
 Cassata, P., Guzzo, L., Franceschini, A., et al. 2007, ApJS, 172, 270
 Cassata, P., Cimatti, A., Kurk, J., et al. 2008, A&A, 483, L39
 Cattaneo, A.; Dekel, A.; Faber, S. M.; Guiderdoni, B., 2008, MNRAS, 389, 567
 Chabrier, G. 2003, PASP, 115, 763
 Charlot & Bruzual 2007
 Cimatti, A., Daddi, E., Renzini, A., 2006, A&A, 453, L29
 Cirasuolo, M., McLure, R. J., Dunlop, J. S., et al. 2007, MNRAS, 380, 585
 Cole, S.; Lacey, C. G.; Baugh, C. M.; Frenk, C. S., 2000, MNRAS, 319, 168
 Cole, S., Norberg, P., Baugh, C. M., et al. 2001, MNRAS, 326, 255
 Coleman, G. D., Wu, C.-C., Weedman, D. W. 1980, ApJS, 43, 393
 Cortese, L.; Gavazzi, G.; Boselli, A.; et al., 2006, A&A, 453, 847
 Cowie, L. L., Songaila, A., Hu, E. M., Cohen, J. G. 1996, AJ, 112, 839
 Cucciati, O., Iovino, A., Marinoni, C., et al. 2006, A&A, 458, 39
 Dekel, A., Birnboim, Y., Engel, G., et al., 2009, Nature, 457, 451
 De Lucia, G., Springel, V., White, S. D. M., Croton, D., Kauffmann, G. 2006, MNRAS, 366, 499
 De Lucia, G., Poggianti, B. M., Aragón-Salamanca, A., et al. 2007, MNRAS, 374, 809
 De Lucia, G., Blaizot, J., 2007, MNRAS, 375, 2
 de Ravel, L.; Le Fèvre, O.; Tresse, L.; et al., 2009, A&A, 498, 379
 Dickinson, M.; Papovich, C.; Ferguson, H. C.; Budavári, T., 2003, ApJ, 587, 25
 Driver, S. P.; Phillipps, S.; Davies, J. I.; et al., 1994, MNRAS, 268, 393
 Drory, N., Salvato, M., Gabasch, A., et al. 2005, ApJ, 619, L131
 Elvis, M.; Civano, F.; Vignali, C.; et al., 2009, ApJ submitted (arXiv:0903.2062)
 Faber, S. M., Willmer, C. N. A., Wolf, C., et al., 2007, ApJ, 665, 265
 Feldmann, R., Carollo, C. M., Porciani, C., et al. 2006, MNRAS, 372, 565
 Felten, J. E. 1976, ApJ, 207, 700
 Feulner, G., Gabasch, A., Salvato, M., et al. 2005a, ApJ, 633, L9
 Feulner, G., Goranova, Y., Drory, N., et al. 2005b, MNRAS, 358, L1
 Fontana, A., Pozzetti, L., Donnarumma, I., et al. 2004, A&A, 424, 23, F04
 Fontana, A., Salimbeni, S., Grazian, A., et al. 2006, A&A, 459, 745

- Fontanot, F.; De Lucia, G.; Monaco, P.; Somerville, R. S.; Santini, P. 2009, MNRAS accepted, (arXiv:0901.1130v2)
- Franzetti, P., Scodreggio, M., Garilli, B., et al. 2007, A&A, 465, 711
- Gavazzi, G., Scodreggio, M., 1996, A&A, 312, L29
- Gehrels, N. 1986, ApJ, 303, 336
- Genzel, R.; Tacconi, L. J.; Eisenhauer, F., et al., 2006, Nature, 442, 786
- Genzel, R.; Burkert, A.; Bouché, N.; et al., 2008, ApJ, 687, 59
- Giallongo, E., Salimbeni, S., Menci, N, et al. 2005, ApJ, 622, 116
- Graves, G. J.; Faber, S. M.; Schiavon, R. P.; Yan, R., 2007, ApJ, 671, 243
- Gwyn, S.D.J., Hartwick, F.D.A., 2005, AJ, 130, 1337
- Juneau, S., Glazebrook K., Crampton, D., et al. 2005
- Hasinger, G., Cappelluti, N., Brunner, H., et al. 2007, ApJS, 172, 29
- Hogg, D.W., Blanton, M., Strateva, I., et al. 2002, AJ, 124, 646
- Hopkins, A. M., Beacom, J. F., 2006, ApJ, 652, 864
- Ilbert, O., Arnouts, S., McCracken, H. J., et al. 2006, A&A, 457, 841
- Ilbert, O.; Salvato, M.; Le Floch, E.; et al. 2009, ApJ submitted (arXiv0903.0102)
- Iovino, A., Cucciati, O., Scodreggio, M., et al. 2009, A&A, submitted
- Kauffmann, G., Heckman, T. M., White, S. D. M., et al. 2003, MNRAS, 341, 33
- Kennicutt, R. C. Jr., 1998, ARA&A, 36, 189
- Kitzbichler, M. G., White, S. D. M., 2007, MNRAS, 376, 2
- Kinney, A. L., Calzetti, D., Bohlin, R. C., et al. 1996, ApJ, 467, 38
- Kodama, T., Yamada, T., Akiyama, M., et al. 2004, MNRAS, 350, 1005
- Koekemoer, A. M.; Aussel, H.; Calzetti, D.; et al., 2007, ApJS, 172, 196
- Kovač, K., Lilly, S.J., Cucciati, O., et al. 2009, ApJ, submitted (astro-ph//arXiv:0903.3409)
- Larson, R. B.; Tinsley, B. M.; Caldwell, C. N., 1980, ApJ, 237, 692
- Le Fèvre, O., Saisse, M., Mancini, D., et al. 2003, SPIE, vol. 4841, p.1670
- Lilly, S. J.; Le Fevre, O.; Hammer, F.; Crampton, D., 1996, ApJ, 460, L1
- Lilly, S.J., Le Fèvre, O., Renzini, A., et al. 2007, ApJS, 172, 70
- Lilly, S.J., Le Brun, V., Maier, C., et al. 2009, ApJS, submitted
- Lin, L., Koo, D. C., Willmer, C. N. A., et al., 2004, ApJ, 617, 9L
- Lo Faro B., Monaco P., Fontanot F. et al. 2009, MNRAS submitted
- Madau, P.; Ferguson, H. C.; Dickinson, M. E.; Giavalisco, M.; Steidel, C. C.; Fruchter, A., 1996, MNRAS, 283, 1388
- Madau, P., Pozzetti, L., & Dickinson, M. 1998, ApJ, 498, 106
- Maier, C.; Lilly, S. J.; Zamorani, G.; et al., 2009, ApJ, 694, 1099
- Maraston, C., Daddi, E., Renzini, A., et al. 2006, ApJ, 652, 85
- Maraston, C., 2005, MNRAS, 362, 799
- Marchesini, D.; van Dokkum, P. G.; Forster Schreiber, N. M.; Franx, M.; Labbe', I.; Wuyts, S., 2008, submitted to ApJ (arXiv:0811.1773v1)
- Menci, N., Fontana, A., Giallongo, E., et al. 2005, ApJ, 632, 49
- Menci, N., Fontana, A., Giallongo, E., et al. 2006, ApJ, 647, 753
- Meneux, B.; Guzzo, L.; de la Torre, S.; et al., 2009, A&A accepted (arXiv0906.1807)
- McCracken, H.J., Capak, P., Salvato, M., et al. 2009, ApJ, submitted
- Mignoli, M., Zamorani, G., Scodreggio, M., et al. 2009, A&A, 493, 39
- Mihos, J. C.; Hernquist, L., 1996, ApJ, 464, 641
- Monaco, P.; Murante, G.; Borgani, S.; Fontanot, F., 2006, ApJ, 652, L89
- Monaco, P., Fontanot, F., Taffoni, G., 2007, MNRAS, 375, 1189
- Moresco, M., et al. 2009, A&A, to be submitted
- Moustakas, J.; Kennicutt, R.C., Jr.; Tremonti, C. A. 2006, ApJ, 642, 775
- Nelan, J. E.; Smith, R. J.; Hudson, M. J.; et al., 2005, ApJ, 632, 137
- Noeske, K. G., Faber, S. M., Weiner, B. J., et al. 2007a, ApJ, 660, L47
- Noeske, K. G., Weiner, B. J., Faber, S. M., et al. 2007b, ApJ, 660, L43
- Norberg, P.; Cole, S.; Baugh, C. M.; et al. 2002, MNRAS, 336, 907
- Oesch P., et al. 2009, ApJ submitted
- Parry, O. H.; Eke, V. R.; Frenk, C. S., 2009, MNRAS, 396, 1972
- Popesso, P., Biviano, A., Bohringer, H., Romaniello, M. 2006, A&A, 445, 29
- Pozzetti, L., Mannucci, F., 2000, MNRAS, 317, L17
- Pozzetti, L., Cimatti, A., Zamorani, G., et al. 2003, A&A, 402, 837
- Pozzetti, L., Bolzonella, M., Lamareille, F., et al. 2007, A&A, 474, 443
- Renzini, A. 2007, in 'At the Edge of the Universe: Latest Results from the Deepest Astronomical Surveys', ed. by J. Afonso, ASP Conf. Ser. 380, 309
- Renzini, A., 2009, MNRAS accepted
- Salpeter, E. E. 1955, ApJ, 121, 161
- Sandage, A., Tammann, G.A., & Yahil, A., 1979, ApJ, 232, 352
- Sanders, D. B., Salvato, M., Aussel, H., et al. 2007, ApJS, 172, 86
- Sargent, M. T., Carollo, C. M., Lilly, S. J., et al. 2007, ApJS, 172, 434
- Scarlata, C., Carollo, C.M., Lilly, S.J., et al. 2007a, ApJS, 172, 406
- Scarlata, C., Carollo, C.M., Lilly, S.J., et al. 2007b, ApJS, 172, 494
- Schechter, P. 1976, ApJ, 203, 297
- Schinnerer, E., Smolčić, V., Carilli, C. L., et al. 2007, ApJS, 172, 46
- Scodreggio, M., Franzetti, P., Garilli, B., et al. 2005, PASP, 117, 1284
- Scoville, N., Aussel, H., Brusa, M., et al. 2007, ApJS, 172, 1
- Schmidt, M. 1959, ApJ, 129, 243
- Schmidt, M. 1968, ApJ, 151, 393
- Skibba, R. A.; Bamford, S. P.; Nichol, R. C.; et al., 2008, MNRAS accepted (arXiv0811.3970)
- Somerville R. S., Hopkins P. F., Cox T. J., Robertson B. E., Hernquist L., 2008, MNRAS, 391, 481
- Strateva, I., Ivezić, Z., Knapp, G.R., et al. 2001, AJ, 122, 1861
- Taylor, Edward N, Franx, Marijn, van Dokkum, Pieter G, et al. 2008, ApJ (in press, arXiv:0810.3459)
- Taniguchi, Y., Scoville, N., Murayama, T., et al. 2007, ApJS, 172, 9
- Tasca, L., Kneib, J.P., Iovino, A., et al. 2009, A&A, in press
- Thomas, D., Maraston, C., Bender, R., Mendes de Oliveira, C., 2005, ApJ, 621, 673
- Toomre, A.; Toomre, J., 1972, ApJ, 178, 623
- van Dokkum, P. G. 2005, AJ, 130, 2647
- Vergani, D., Scodreggio, M., Pozzetti, L., et al. 2008, A&A, 487, 89
- Vergani, D., Zamorani, G., Lilly, S., et al. (2009), A&A submitted
- Walcher, C. J.; Lamareille, F.; Vergani, D.; et al., 2008, A&A, 491, 713
- Wang, L.; Kauffmann, G., 2008, MNRAS, 391, 785
- Wang J., De Lucia G., Kitzbichler M. G., White S. D. M., 2008, MNRAS, 384, 1301
- Weiner, B.J., Phillips, A.C., Faber, S.M., et al. 2005, ApJ, 620, 595
- Williams, R. J., Quadri, R. F., Franx, M., van Dokkum, P., Labbé, I., ApJ, 691, 1879
- Zamojski, M. A., Schiminovich, D., Rich, R. M., et al. 2007, ApJS, 172, 468
- Zucca, E., Zamorani, G., Vettolani, G., et al. 1997, A&A, 326, 477
- Zucca, E., Ilbert, O., Bardelli, S., et al. 2006, A&A, 455, 879
- Zucca, E., Bolzonella, M., Bardelli, S., et al. 2009, A&A submitted

¹ INAF – Osservatorio Astronomico di Bologna, via Ranzani 1, I-40127, Bologna, Italy

² Institute of Astronomy, Swiss Federal Institute of Technology (ETH Hönggerberg), CH-8093, Zürich, Switzerland

³ Dipartimento di Astronomia, Università di Padova, Padova, Italy

⁴ Dipartimento di Astronomia, Università degli Studi di Bologna, via Ranzani 1, I-40127, Bologna, Italy

⁵ Department of Astronomy, University of Massachusetts, 710 North Pleasant Street, Amherst, MA 01003, USA

⁶ Laboratoire d'Astrophysique de Marseille, Université d'Aix-Marseille, CNRS, 38 rue Frederic Joliot-Curie, F-13388 Marseille Cedex 13, France

⁷ INAF – Istituto di Astrofisica Spaziale e Fisica Cosmica di Milano, via Bassini 15, I-20133 Milano, Italy;

⁸ Laboratoire d'Astrophysique de Toulouse-Tarbes, Université de Toulouse, CNRS, 14 avenue Edouard Belin, F-31400 Toulouse, France

⁹ Max Planck Institut für Extraterrestrische Physik, D-84571 Garching, Germany

¹⁰ INAF – Osservatorio Astronomico di Brera, via Brera 28, I-20121 Milano, Italy

¹¹ INAF – Osservatorio Astrofisico di Arcetri, Largo Enrico Fermi 5, I-50125 Firenze, Italy

¹² Space Telescope Science Institute, 3700 San Martin Drive, Baltimore, MS 21218, USA

¹³ Centre de Physique Theorique, Marseille, Marseille, France

¹⁴ Institut d'Astrophysique de Paris, Université Pierre & Marie Curie, Paris, France

- ¹⁵ INAF – Osservatorio Astronomico di Roma, via di Frascati
33, I-00040 Monteporzio Catone, Italy
- ¹⁶ Spitzer Science Center, Pasadena, CA, USA
- ¹⁷ California Institute of Technology, MC 105-24, 1200 East
California Boulevard, Pasadena, CA 91125, USA